Mohamed Khider University of Biskra
Faculty of exact sciences and natural and life sciences
Material sciences department

MASTER MEMORY

Domain of Matter Sciences
Section of Physics
Specialty of Energetic Physics and Renewable Energies.

Réf. :Entrez la référence du document

Presented by:
AMRAOUI Fatma and GHARBI Imane

Le :19/6/2022

The Influence of Calcination Temperature on Properties of Thin films of Zinc-Oxide (ZnO) elaborated by Sol-gel (Dip-coating)

Jury:

Mrs	Hamani Nadjette	MCB	University of Biskra	President
Mr	Saâd Rahmane	Professor	University of Biskra	Supervisor
Mrs	Kater Aicha	MCA	University of Biskra	Examiner

Academic Year: 2021\2022

DEDICATED

To our family and friends

To our teachers and colleagues

ACKNOWLEDGEMENT

Inspiration and motivation have always a key role in the success of any venture. First and foremost, praises and thanks to God, the almighty, for his showers of blessings throughout our research work to complete it successfully.

We would like to express our gratitude and appreciation to all those who gave us the possibility to complete this project.

Special thanks to our supervisor **Pr. Saâd RAHMANE** for his support in completing the project. His constant guidance and willingness to share his vast knowledge made us understand this project, his patience and encouragement that carried us on through difficult times and helped us to complete the assigned tasks on time.

We are highly indebted to **Dr. KATER Aicha** for her valuable guidance which has prompted our efforts in all the stages of our studies, and agreed to accept to belong to the jury and to examine our work.

We are grateful to **Pr. GHETTAF TEMAM Elhachmi** for his continuous guidance advice effort and his supports during the experimental part.

We address our sincere thanks to **Dr. HAMANI Nadjette** for the honor that makes to us by accepting the presidency of this jury.

We would like to thank **Pr. TIBERMACINE Toufik** for all the electrical measurements made on our thin films.

We are also thankful to **Dr. BELHAMRA Feriel** for her constant encouragement and her help extended to our work.

Our thanks and appreciation go to **Pr. BEN TAMAM Hachemi** the head chef of laboratory of **Physics of Thin Films and Applications** in Mohamed Khider university, and all the members and staff who have willingly helped us out with their abilities in this laboratory.

Table of contents:

Chapter III: Experimental details and discussion.

GENERAL INTRODUCTION

GENERAL INTRODUCTION

Historically, thin films have been used for more than a half century in making electronic devices, optical coatings, instrument hard coatings, and decorative parts. The thin film is a traditional well-established material technology. However, thin film technology is still being developed on a daily basis since it is a key in the twenty-first century development of new materials such as nanometer materials.

Thin film materials and devices are also available for minimization of toxic materials since the quantity used is limited only to the surface. Thin film processing also saves on energy consumption in production and is considered an environmentally benign material technology for the next century [1].

One of interested thin films is TCOs, transparent conductive oxides, due to its wide variety of uses and high performance of electronic devices (such as zinc oxide (ZnO) [2], indium oxide (In_2O_3) [3], tin oxide (SnO_2) [4] ..., etc). TCOs are materials which combine optical transparency with electrical conductivity. In order to obtain a transparent material, they must display a band gap greater than the highest frequency of visible light (3.1 eV). Metals for instance are highly conductive but do not transmit visible light and transparent materials such as glasses are insulators. TCOs exhibit intrinsic conductivity due to defect states in the crystal structure [2]. In addition, it is well known that TCO of zinc oxide has attracted the attention of many researchers, simply because of its important properties.

Zinc oxide is a wide band gap compound semiconductor ($E_g = 3.2$ eV), which has been investigated as an electronic material for many decades, starting in the 1930s. It has a high optical transparency to the visible light; thus, it belongs to the class of transparent conducting oxides (TCO). Recently, fundamental and applied research on zinc oxide experienced a renaissance due to the prospective use of zinc oxide as an optoelectronic material for blue and UV lasers. Moreover, ZnO thin films are important components in most thin film solar cells [5].

A deposition technique is considered as the integral key for the creation of thin film new materials to meet the ever-increasing demand from industries for versatile and multi-dynamics materials. The deposition techniques determine virtually all the properties of the thin film and can be used to modify the existing properties [6].

ZnO thin films can be deposited by serval techniques such as CVD (chemical vapor deposition) [7], reactive magnetron sputtering [8], Sol-Gel [9] … etc. Among these methods, Dip-coating technique by sol-gel method was selected to deposit ZnO thin films due to many benefits could be offered such as simplicity, needless of heavy equipment and other advantage will be discussing later.

The objective of this work is to control the synthesis of zinc oxide films elaborated by the dip-coating technique, and to study the influence of calcinations temperature on the structural, optical and electrical properties of these films in order to optimize these parameters, to obtain ZnO thin films with good quality.

In addition to a general introduction to the subject, the manuscript consists of three chapters:

The first chapter presents a review of the thin films and the various deposition methods, a bibliographic overview of transparent conductive oxides (TCO), also a brief survey on ZnO and its properties. In addition, a review of doped zinc oxide thin films and zinc oxide applications.

The second chapter gives the definition of Sol-Gel process, and then we describe dip-coating method and characterization tools used to define the properties of thin films (structural, morphological, optical and electrical properties).

The third chapter is devoted to study the influence of calcinations temperature on ZnO thin films properties. It contains the experimental details of film deposition procedures with results and discussion.

Finally, we present general conclusion including the most important results obtained in this work.

REFERENCES

[1] K. Wasa, M. Kitabatake, H. Adachi. Thin Film Materials Technology: sputtering of compound materials, springer science & business media. (2004),518 pages.

[2] D. S. Bhachu, the synthesis and characterization of metal oxide thin films, doctoral thesis, UCL (University College London), (2013).

[3] M. Qin, J. Ma, W. Ke, P. Qin, H. Lei, H. Tao, X. Zheng, L. Xiong, Q. Liu, Z. Chen, Perovskite solar cells based on low-temperature processed indium oxide electron selective layers, ACS Appl. Mater. Interfaces. 8 (2016) 8460‑8466.

[4] Z. Chen, W. Li, R. Li, Y. Zhang, G. Xu, H. Cheng, Fabrication of highly transparent and conductive indium−tin oxide thin films with a high figure of merit via solution processing, Langmuir. 29, 13836−13842, (2013).

[5] E. Klaus, A. Klein, B. Rech, Transparent conductive zinc oxide: basics and applications in thin film solar cells. Springer-Verlag, Berlin Heidelberg, (2008).

[6] Ola. Oluwatosin Ab. egunde, E. Tit.Akinlabi, Olu. Ph.Oladijo, St. Akinlabi, Al. Uchenna Ude, Overview of thin film deposition techniques, AIMS Materials Science, 6(2) (2019) 174-199.

[7] Z. Guangyao, G. Shulin, Z. Shunming, S. Huang, R. Gu, J. Ye, Y. Zheng. Optimization study of metal-organic chemical vapor deposition on sapphire substrate, Journal of Crystal Growth 349, 6-11, (2012).

[8] J.Lee , D. Lee, D. Lin, K. Yang, Structural, electrical and optical properties of ZnO: Al films by deposited on flexible organic substrates for solar cell applications. Journal Thin solid films 515,6094-6098, (2007).

[9] K.A Vijay, S.C. Sood, Anurekha.S, Characterization of ZnO Thin Film Deposited by Sol-Gel Process, AIP Conference Proceedings 1324, 399, (2010).

Chapter I:

Bibliographic research.

I.1 Introduction:

During the last few years, zinc oxide (ZnO), which is one of the most important binary II–VI semiconductor compounds, have attracted the interest of many research groups due to it is application in light emitting diodes (LEDs), laser diodes, and optoelectronic, device material for use in the violet and blue regions considering it is wide band gap $(3.37\ eV)$ large exciton binding energy $(60\ meV)$ at room temperature [1].

This chapter is devoted to discuss the thin films and their deposition techniques, and with providing a bibliographic overview of transparent conductive oxides (TCO).

We will also present zinc oxide (ZnO), including it is structural, optical and luminescence, electrical and electronic properties. Review of doped zinc oxide thin films and zinc oxide applications.

I.2 Thin films:

The thin film can be labeled as thin materials layers ranging from a fraction of nanometers to one micron $(10^{-6}\ meters)$ in thickness. The paramount distinction between thin film and thick coating depositions is the thickness of the layers deposited. Thin film deposition involves deposition of individual atoms or molecules on the surface while thick coating deals with deposition of particles. It is being used to modify the physical, chemical properties and surface morphology of materials without altering the properties of the bulk material.

A thin film can be personalized as one homogeneous composition, single layer, crystalline phase composition, and microstructure, or it has an inhomogeneous multilayer or/and composite structure depending on the envisaged properties and area of applications. The multilayer's structure can be periodic; it has a set pattern or be entirely random. Almost all thin films deposition techniques have four or five basic chronological steps. The steps are unique to the overall properties of the thin film and are listed below [2,3]:

- The source of the pure material to be dispatched is selected. This source of material will act as a target during the deposition process.
- The target is transported through a medium to the prepared substrate. This medium can either be a fluid or vacuum, depending on the materials and the deposition technique used.

- The target is deposited onto the substrate, forming a thin film on the substrate surface. The thin film may be subjected to an annealing or other heat treatment process, depending on whether or not this is necessary to achieve the desired film properties.
- The film properties are analyzed, if necessary, the analysis results can be incorporated to modify the deposition process.

Generally, thin films are fabricated by the deposition of individual atoms on a substrate [4], and they are defined as a low-dimensional material created by condensing one-by-one atomic/molecular/ionic species of matter, the thickness is typically less than several microns [5].

I.2.1 Thin films growth process:

Thin films are deposited on a substrate by thermal evaporation, chemical decomposition, and/or the evaporation of source materials by the irradiation of energetic species or photons.

Any thin-film deposition process involves three main steps:

- Production of the appropriate atomic, molecular, or ionic species.
- Transport of these species to the substrate.
- Condensation on the substrate, either directly or via a chemical and/or electrochemical reaction, to form a solid deposit.

The unit species, on impacting the substrate, lose their velocity component normal to the substrate (provided the incident energy is not too high), and they are physically adsorbed on the substrate surface. The adsorbed species are not, initially, in thermal equilibrium with the substrate initially and move over the substrate surface. In this process, they interact among themselves forming bigger clusters.

The clusters or the nuclei, as they are called, are thermodynamically unstable and may tend to desorbs in time, depending on the deposition parameters.

If the deposition parameters are such that a cluster collides with other adsorbed species before getting desorbed, it starts growing in size. After reaching a certain critical size, the cluster becomes thermodynamically stable, and the nucleation barrier is stated to have been overcome, this step involving the formation of stable, chemisorbed, and critical-sized nuclei is called the nucleation stage.

The critical nuclei grow in number as well as in size until a saturation nucleation density is reached. The nucleation density and the average nucleus size depend on a number of parameters such as: the energy of the impinging species, the rate of impingement, the activation

energies of adsorption, desorption, thermal diffusion, the temperature, topography, and chemical nature of the substrate.

A nucleus can grow both parallel to the substrate by surface diffusion of the adsorbed species, and perpendicular to it by direct impingement of the incident species. However, the rate of lateral growth at this stage is much higher than the perpendicular growth, mostly. The grown nuclei are called islands.

The next stage in the process of film formation is the coalescence stage, in which the small islands start coalescing with each other in an attempt to reduce the substrate surface area. This tendency to form bigger islands is termed agglomeration; it is enhanced by increasing the surface mobility of the adsorbed species.

Larger islands grow together, leaving channels and holes of uncovered substrate. The structure of the films at this stage changes from discontinuous island type to porous network type, filling of the channels and holes forms a completely continuous film [6,7].

I.2.2 Growth modes:

In the early stage of research on thin films, it soon became clear that it was imperative to understand the mechanisms, which control and define the thin films'growth in order to realize good control over these novel materials. Hence the huge effort of the scientific community to characterize, optimize and comprehend film growth.

Evidently, thin films are composed of atoms, which are their zero-dimensional building blocks. Extending this concept, nanoparticles (also termed 'nano-crystals') can also serve as zero-dimensional building blocks which by self-assembly may form two-dimensional thin films or three-dimensional crystals (so-called 'nanoparticle super-lattices'), analogous to atomic films and crystal lattices [6].

Atomic thin film growth is understood to occur in form of three basic growth modes, which result from competing energy terms during the film deposition, i.e. Frank van der Merwe, Stranski-Krastanov, and Volmer-Weber growth. Various processes occur when atoms arrive at a substrate during thin film growth.

That are adsorption, desorption, diffusion, finding or leaving of equilibrium positions. These processes occur simultaneously averaged over the ensemble of arriving atoms [8-10].

As in the case of atoms, the interplay of various free energy terms determines the way on how the nanoparticles (NPs) films will grow. These are in detail [11]: an entropic contribution

E_{TS}, an inter-particle energy term E_P, summing up all relevant types of interactions between NPs [12], and a NP-to-substrate interaction energy E_S. A further significant factor is the diffusion energy barrier E_d that can be overcome by 'thermal' energy k_BT_S. Hereby T_S is a quantity comparable to a substrate 'temperature', which precise physical meaning still requires to be understood for NP systems.

Depending on the relative magnitudes of E_d and k_BT_S, the NPs will either stay fixed at one place once they are attached to the substrate or move freely to seek energetically more favorable locations considering the two extreme cases.

From a comparison of these free energy terms one finds [10,11], that three different growth modes follow: in the case where NP to substrate energy, Es dominates a layer-by-layer growth is found, viz. the so-called Frank-van-der-Merwe growth mode.

Once a stable cluster (or 'nucleus') of NPs is formed, the following NPs prefer to attach at the periphery of the nucleus in contact with the substrate.

Accordingly, this leads to the advancement of planar film growth, depending on the ratio of E_d and k_BT_S (i.e. the mobility of NPs) one will obtain either polycrystalline or single-crystalline superlattices.

In the first case, the immobility of NPs leads to the nucleation of many independent super lattice crystallites while, in the other case, the large mobility enables the NPs to seek equilibrium positions and hence it promotes single-crystal growth [7].

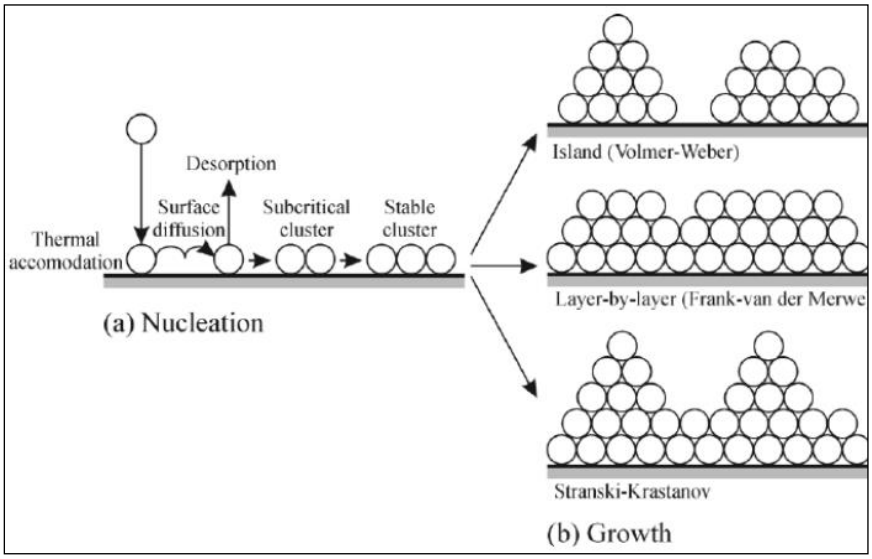

Figure I-1: Schematic representation of: (a) the steps leading to nucleation, (b) the three film growth modes [13].

I.3 Thin film deposition techniques:

I.3.1 Physical vapor deposition (PVD):

Physical Vapor deposition techniques are the range of techniques used to deposit thin films onto a substrate using purely physical processes. PVD processes are environmentally friendly vacuum deposition techniques consisting of three fundamental steps:

- Vaporization of the material from a solid source assisted by high temperature vacuum or gaseous plasma.
- Transportation of the vapor in vacuum or partial vacuum to the substrate surface.
- Condensation onto the substrate to generate thin films [14].

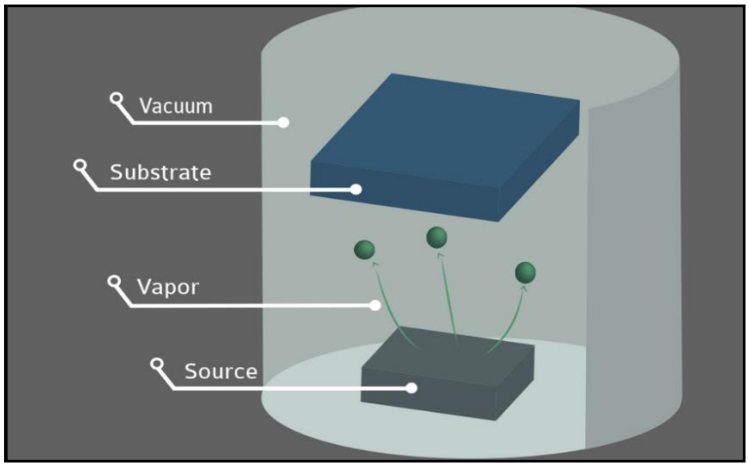

Figure I-2: Physical vapor deposition method [15].

Physical vapor deposition (PVD) mainly includes evaporation, spraying in all its forms, and laser ablation [16]. The most widely used PVD methods are Thermal (or vacuum) evaporation, and sputtering [5].

I.3.1.1 Thermal (or vacuum) evaporation:

Thermal (or vacuum) evaporation is an old deposition process used for the formation and growth of the thin film on the solid materials' surface. The process is still beneficial in a contemporary environment and extensively applicable in the laboratory and industries for deposition of the thin film.

The basic sequential steps for thermal or vacuum evaporation are provided below:

- The vapor is created from subjecting the target material to very high temperature by subliming or boiling.

- The ejected vapor from the target material is transported to the substrate through a vacuum.
- Condensation of the vapor takes place to form a solid thin film on the substrate's surface, and further repeatability of the deposition cycles result in thin film growth and nucleation [17].

During the thermal evaporation process, the target material vaporized from the thermal process sources gets to the substrate material with minimal interference. The process is often carried out at a high vacuum pressure, and the trajectory of the movement of the target material to the substrate is a straight path trajectory termed line of sight [2].

Vapor flux is created by heating the surface of source material to a sufficiently elevated temperature in a vacuum; the flux can then condense to the surface of the substrate material to form a thin film.

The vacuum environment creates a safe zone to reduce gaseous contaminants in the deposition process to an acceptable and minimal level; it allows the evaporated atoms to undergo essentially collision less transport from the source onto the substrate.

The gas pressure range is usually between (0.0013 Pa to 1.3×10^{-9} Pa) depends on the degree of the contamination in the deposition system, with the mean free path (MFP, the average distance between collisions occurring between species) no smaller than 5 mm.

The thermal vaporization rate might be very high compared to other (PVD) processes, 'Tungsten' wire coils are commonly used as the source of the thermal heat or by using high energy electron beam for heating the target material to an elevated temperature.

Evaporation process has been reported to be performed using different configurations, these are Molecular beam epitaxy, reactive evaporation and activate reactive evaporation [2,18].

I.3.1.2 Sputtering:

Sputtering is a vital and prominent procedure among the PVD processes. It is a non-thermal vaporization process whereby individual atom escapes from the target surface due to atomic collision cascades by suitable high-energy ion bombardment [19].

The sputtering deposition has become a generic name for a variety of sputtering processes; these processes are named based on their source and the orientation of the process. Variants of sputtering are diode sputtering (cathode or radio frequency), reactive sputtering, bias sputtering, magnetron sputtering, and ion-beam sputtering [20].

Sputtering deposition technique employs various sources for power, and the working pressure varies depending on the power configuration.

DC sputtering is made up of a pair of planar electrodes (referred to as the cold cathode and anode), the target material to be deposited is placed on the cathode, and the substrate is positioned at the anode.

The working gas inside the deposition chamber is usually argon gas because of the larger mass compared to neon and helium since higher mass correlates to more energetic collision with the target material and lower cost when compared to xenon and krypton.

DC voltage is supplied between the cathode (target material) and anode (substrate) to sustain the glow discharge. The gaseous ions resulted from the sustained glow discharges are accelerated towards the target material, and sputtering takes place resulting in deposition of a thin film on the surface of the substrate material. In the DC sputtering system, the target is composed of conducting material usually metal since the glow discharge (current flow) is maintained between the metallic electrodes [21,22].

Radio Frequency (RF) sputtering is another variant of sputtering which includes alternating the electrical potential of the current in the vacuum environment at radio frequencies to avoid charge building up on certain types of sputtering target materials. In RF sputtering, the cathode (the target) which is to become the thin film coating and an anode is connected in series with a blocking capacitor in between. The capacitor is part of an impedance-matching network that provides the power transfer from the RF source to the plasma discharge. The cathode is bombarded by high voltage in a vacuum chamber leading to high-energy ions sputtering off atoms as a thin film covering the substrate to be coated at a fixed frequency of 13.56 MHz .

The essence of the capacitor is to develop DC self-bias and enlarge the optimization of power transfer for the target material to the plasma generated.

RF sputtering offers numerous advantages like possibility of deposition on insulating materials, ability to sustain plasma at low pressure of 0.13 to 2 Pa.

Diffusion of RF plasma throughout the entire chamber, reduction of the creation of racetrack erosion on the surface of the target, and ability to clean up the target materials after each cycle from building up charge to reduce arcing effect [23,24].

Conductive materials can be deposited using a direct current (DC) power supply and insulators can be deposited by using a radio frequency (RF) power supply, Magnetic arrays in

magnetron sputtering configuration can be varied in situ without tempering with the electromagnet [17].

I.3.2 Chemical vapor deposition (CVD):

CVD is a thermodynamically complex process consisting of chemical reactions under specific conditions such as temperature, pressure, reaction rates, momentum, mass, and energy transport.

Several process factors and chemical reaction between the reactant and substrate are responsible for the quality of films produced during CVD, and the quality of the film can be controlled and modified by using the appropriate combination of process parameter like: flow rates, pressure, temperature, concentration of chemical species, and reactor geometry [17].

The CVD process can be summarized in five steps:

- Transporting reactive gas species (or species) to the substrate.
- Adsorption of the reactants on the surface.
- Surface reaction and film growth.
- Desorption of volatile secondary products.
- Transport and evacuation of gaseous products to the reactor outlet.

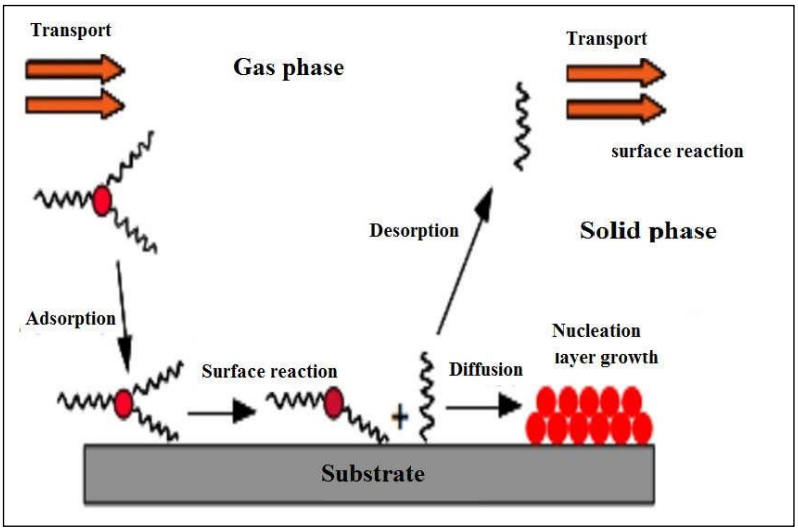

Figure I-3: The main steps of deposition by the CVD method [16].

The improvement of this technique is to diminish the deposition temperature and the reactor pressure and remedy the low volatility of the precursors.

Several CVD type techniques can be given [25]:

- APCVD: (Atmospheric Pressure Chemical Vapor Deposition) deposition under atmospheric pressure.

- LPCVD: (Low-Pressure Chemical Vapor Deposition) low-pressure deposition.
- MOCVD: (Metal Organic CVD) the use of organ metallic precursors.
- PACVD: (Plasma Assisted Chemical Vapor Deposition) with the assistance of a plasma.

I.3.3 Spray pyrolysis technique:

The spray pyrolysis is a simple technique based on chemical vapor deposition process (CVD). In this technique, the precursor of the material to be deposited is in solution and sprayed onto a heated substrate using air as carrier gas [26]. The method has been employed for the deposition of dense films, porous films, and for powder production. Even multi-layered films can be easily prepared using this versatile technique. Spray pyrolysis has been used for several decades in the glass industry and in solar cell production.

Typical spray pyrolysis equipment consists of an atomizer, precursor solution, substrate heater, and temperature controller. The following atomizers are usually used in spray pyrolysis technique: air blast (the liquid is exposed to a stream of air), ultrasonic (ultrasonic frequencies produce the short wave length necessary for fine atomization), and electrostatic (the liquid is exposed to a high electric field) [6].

The major advantages of spray pyrolysis are that the coatings are more durable than vacuum-deposited coatings, the variety of precursors could be used, and the process can be employed at lower cost than CVD or vacuum deposition.

The disadvantage is that the coatings are not uniform in thickness. CVD consists of vaporizing the precursors and directing the resultant gases onto a hot substrate [14].

In general, case of spray pyrolysis deposition is indicated in Figure I-4:

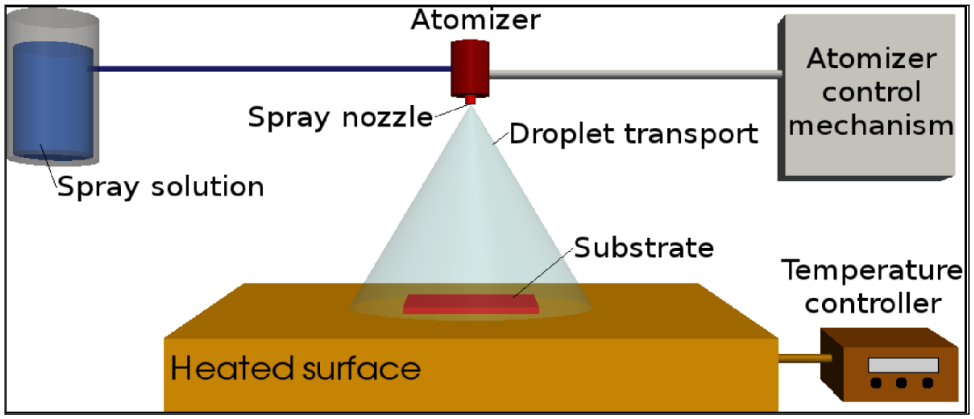

Figure I-4: General schematic of a spray pyrolysis deposition process [14].

I.3.4 Sol gel method:

The sol-gel method is a wet-chemical synthesis technique for preparation of oxide gels, glasses, and ceramics at low temperature [7]. It was developed in the 1960s mainly due to the need of new synthesis methods in the nuclear industry. A method was required where dust was reduced (compared to the ceramic method), and which needed a lower sintering temperature. In addition, it should be possible to do the synthesis by remote control [27].

The sol-gel method is considered effective to modify the surface of substrates. The obtainment of a high surface and the stable surfaces are essentially the most significant advantage of the sol-gel method. The chemical and physical properties of the materials gained by the sol-gel method are related to the experimental conditions applied [28]. It is possible to fabricate ceramic or glass materials in a variety of forms, such as ultra-fine powders, fibers, thin films, porous aerogel materials or monolithic bulky glasses, and ceramics. Since then, powders, fibers, thin films, and monolithic optical lens have been made from the sol-gel glass [26].

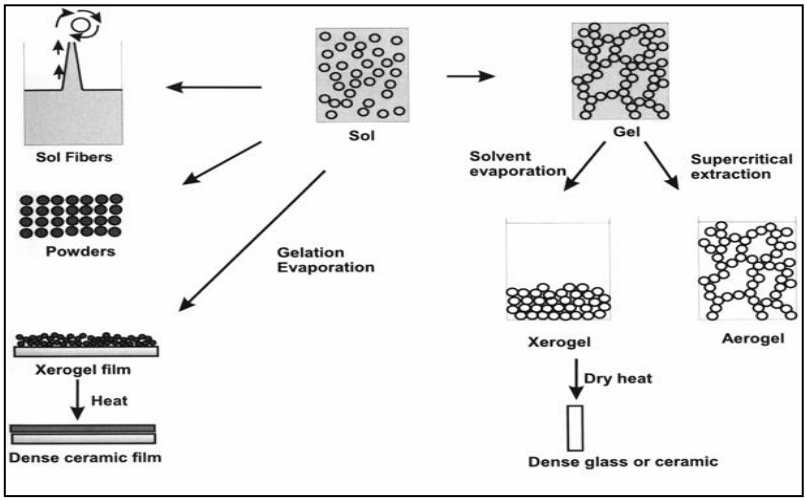

Figure I-5: Synthesis of various forms of materials by the sol-gel method [27].

In the field of research, the thin layers prepared by the sol-gel process are widely known and used in various applications. The most used techniques are dip coating and spin coating.

I.3.4.1 Dip Coating:

The dip coating technique can be described as a film deposition process [26]. A simple, flexible, and cost-efficient coating technique allows the application of a variety of oxide and inorganic-organic hybrid materials [29].

Dip coating has been extensively utilized for research purposes owing to it being a convenient and facile approach. The quality of the coatings produced by this way, nonetheless, is

inconsistent. Therefore, it is an in appropriate approach for industrial processes. The critical parameters that can affect the coatings produced by dip coating.

Dip coating consists of a five-step process, including:

- Immersion: At a constant speed, the substrate is dipped into the coating solution. Based on the kind of the substrate, a pretreatment process would be carried out before this step.
- Startup: The substrate remains in the solution for a designated time, and then it starts to be pulled out.
- Deposition: While the substrate is being pulled out, the thin film coating starts to be deposited on it. The thickness of the coating is directly dependent on the speed by which the substrate is being pulled out. The slower pull, the thinner the coating layer.
- Drainage: In this step, excess liquid is drained from the substrate surface.
- Evaporation: Solvent starts to evaporate from the surface of the substrate to form a thin film. If the solvent is volatile, this step might happen in the deposition (step 3), shown in Figure I-6.

Because no sophisticated equipment is required for this method, it is much more convenient and facile than the other approaches. The coating layer produced; nevertheless, it may not be of good quality, due to the simplicity of the method. The thickness distribution may be an issue. The coating layer produced might not be sufficiently dense to show superior properties, the applied substrate cannot be vastly large and complicated, as well as.

However, dip coating can still be utilized at large scale to produce products fulfilling low standard requirements at a competitive price, although it is more appropriate for use in the lab [30].

We also mention, there are five forces in the film deposition region governing the thickness of the film and the position of the streamline [31]:

1) Viscous drag upward on the liquid by the moving substrate.
2) Force of gravity.
3) Resultant force of surface tension in the concavely curved meniscus.
4) Inertial force of the boundary layer liquid arriving at the deposition region
5) Surface tension gradient.

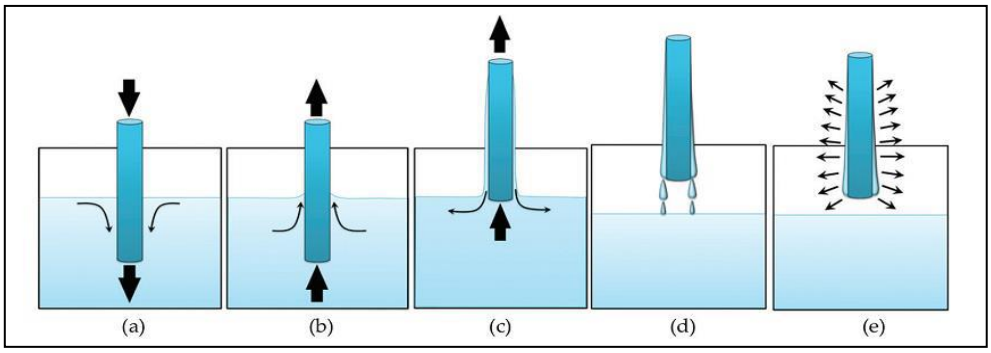

Figure I-6: Dip-coating stages: (a) immersion; (b) start-up; (c) deposition; (d) drainage; (e) evaporation [32].

I.3.4.2 Spin Coating:

Spin coating is used for the thin films' fabrication to deposit uniform coating of organic materials on flat surfaces [33]. This method consists of centrifuging a solution deposited in excess on a substrate. It has the advantage of being easily implemented, and it provides very good results on flat substrates of small areas (a few cm^2) for moderate investments. We can distinguish four main steps in this technique, as presented in Figure I-7.

i. The deposition of the solution.
ii. At the start of the rotation, the acceleration phase causes the liquid to flow towards the outside of the support.
iii. The constant speed rotation allows the ejection of excess liquid in the form of droplets and the reduction of the thickness of the film uniformly.
iv. Evaporation of the more volatile solvents, which enhances the reduction in the thickness of the deposited film [16].

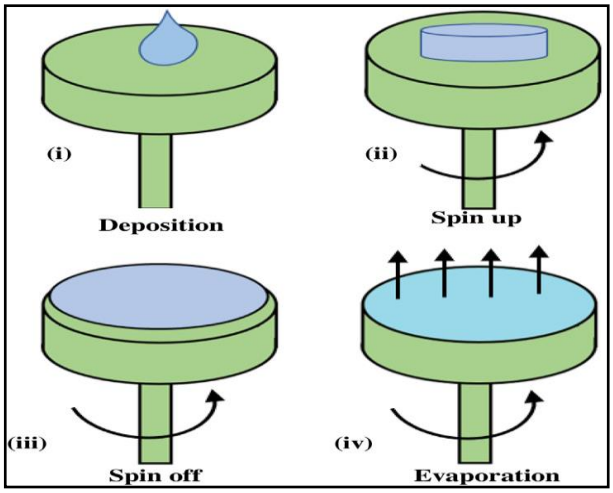

Figure I-7: four steps of spin coating [33].

Final film thickness and other properties will depend on the nature of the fluid material (viscosity, drying rate, percent solids, surface tension...) and the parameters chosen for the spin

process. Factors such as final rotation speed, acceleration, and fume exhaust affect the properties of the coated films [14].

One of the main disadvantages of spin coating is the size of the substrate. As the size increases, the high-speed spinning becomes difficult, because film thinning becomes difficult. The material efficiency of spin coating is very low. In general, 95% to 98% of material is flung off, and disposed of during the process and only 2% to 5% of material is dispensed onto the substrate [33].

I.4 Transparent conductive oxides (TCOs):

Transparent conducting oxides (TCOs) constitute a unique class of materials, which combine two physicals' properties together, high optical transparency and high electrical conductivity. These properties are generally considered to be mutually exclusive for each other since high conductivity do metals possess a property while insulators are optically transparent. This peculiar combination of physical properties is achieved by generating free electron or hole carriers in a material having a sufficiently large energy band gap $(\text{i.e.}, > 3.1\ eV)$ so that it is non-absorbing or transparent to visible light [26].

The general requirements of a TCO thin film, for practical use are a resistivity ($< 10^{-3}\ \Omega.\text{cm}$), and a transmittance of ($> 80\ \%$) in visible range. Badeker published the first report on TCO in 1907 [34]. He reported that thin films of Cadmium metal deposited in a glow discharge chamber could be oxidized to become transparent while remaining electrically conducting. Since then, the commercial value of these thin films has been recognized, and the list of potential TCO materials has expanded to include Aluminum doped ZnO, SnO_2, Fluorine doped In_2O_3, etc.

Most of the research to develop highly transparent and conducting thin films has focused on n-type semiconductors, consisting of metal oxides [32]. Tin-doped indium oxide (ITO) is the most used, for the majority of applications (solar cells, flat screens ...) for a long time, but the cost and the abundance of indium pushed the researchers to seek for a material that maybe a substitute for ITO. Doped and undoped zinc oxide (ZnO) has emerged as a better candidate for its greater transparency in the visible and low resistivity comparable to those of thin layers of ITO, also for its low cost, abundance, and non-toxicity [16].

Historically, TCO films composed of binary compounds, which were developed by means of physical and chemical deposition methods. One of the advantages of using binary compound as TCO material is that their chemical composition in film deposition is relatively easier to

control than that of ternary and multi component oxides. Until now, undoped and impurity doped films such as SnO_2, In_2O_3, ZnO, CdO were developed. These materials have a free electron concentration of the order of 10^{20}cm^{-3} provided by native donors such as oxygen vacancies and interstitial metal atoms. Since impurity doped materials can use both native and impurity donors, undoped binary materials have got limited range of applications.

In addition to these binary compounds, ternary compounds such as Cd_2SnO_4, $CdSnO_3$, and $CdIn_2O_4$ were also developed prior to 1980. As well as, multi component oxides composed of combinations of these ternary compounds were developed. The advantage of the multi component oxide materials is the fact that their electrical, optical, chemical, and physical properties can be controlled by altering their chemical compositions [32].

I.4.1 Electrical and optical properties of TCOs:

Most TCOs are binary or ternary compounds that contain one or two metallic elements. Their resistivity should be as low as $(10^{-4}\Omega.\text{cm})$, and the extinction coefficient in the visible light should be lower than (1×10^{-3}) because of their wide band-gap, which can be greater than $(3\ \text{eV})$.

This amazing combination of conductivity and transparency is usually not viable in intrinsic stoichiometric oxides that are typically very good insulators with $(\rho > 10^{10}\Omega.\text{cm})$ due to the large band-gap $(> 3\ eV)$, which separates the valence band (VB) from the conduction band (CB).

Therefore, the CB cannot be thermally populated at room temperature $(\text{KT}\sim 0.03\ \text{eV})$. In these oxides, a high conductivity is realized by achieving a non-stoichiometric composition or by introducing appropriate dopants. Therefore, the properties of semiconducting oxides strongly depend on the electronic structure, including defect states lying in between the CB and VB (sub-band-gap states) [35].

Although, While TCOs have already found wide spread use in device applications requiring a transparent contact. However, the results obtained are insufficient, and there are currently enormous efforts to increase the conductivity of the existing materials and finding other alternatives.

These efforts are dependent on a microscopic identification of the defects and impurities leading to the high unintentional carrier densities present in these materials. While oxygen

vacancies are commonly assumed the source of the conductivity, there is increasing evidence that this is not a sufficient mechanism to explain the total measured carrier concentrations [36].

The optical properties depend on the interaction of the electromagnetic wave with the electrons of the material. When applying the dispersion theory to the processing of a material, it is important to separate the fundamental absorption from the absorption of the free carriers.

If only the first contribution predominates, the material is a dielectric. In contrast to the second case, the material is a metal. For semiconductors, both contributions are important. The first corresponds to the inter-band absorption threshold and separates the UV absorption region. The region with high transparency in the visible. The second defines the rising edge of Infrared reflection corresponding to the plasma oscillations of the electrons of conduction [34].

The charge carriers are usually generated by doping the insulator with suitable dopants and by defects. It is no wonder that this unique material property makes TCOs an important material in technology and useful in commercial applications [26].

I.4.2 Criteria for choosing TCOs:

The quantitative assessment of the performance of a TCO is given by the quality factor φ_{TC} (merit factor or figure of merit) which is defined by $\varphi_{TC} = T^{10}/R_S$; where T is the optical transmission and R_s is the electrical sheet resistance [37].

It should be noted that the figure of merit gives a good estimate of the TCO's performance of the same microstructure, but there are other parameters that determine the choice of a TCO such as, the stability of TCO [16].

Other parameters relating to the material are, its toxicity, etching properties and its production costs. In the domain of thin films, the frequency of the plasma, the homogeneity of the deposit, and its surface roughness, the stabilities thermal, chemical and mechanical, adherence to the substrate, and heat treatments minimum necessary are also crucial. Finally, the surface properties of TCOs can play a decisive role in the optoelectronic devices performance [38].

I.4.3 Applications of TCOs:

TCOs are materials with high transparency in the visible region and good conductivity and for this coexistence of electrical and optical properties. Such materials have been attracted more intentionally in research and industry; they are the basis of many applications and various components.

- Solar cell
- Optoelectronic systems
- Gas sensors
- Touch screens
- Flat screens
- Electrochromic mirrors and windows
- Windows reflecting heat (buildings, ovens ...)

Although they are used in many applications as mentioned above, TCOs are missing in the application of active devices, because of the need of a p-n junction and most TCOs are n-type; there is considerable research on the type p which are recently reported. The first p-type (NiO) is reported by Sato and al. in 1993 [16].

I.5 Zinc oxide (ZnO):

ZnO is not “a new semiconductor”. It has a long history of studies of its techniques growth and characterization of its material properties. It has been investigated already in 1912. With the beginning of semiconductors age after the invention of the transistor, lattice parameters of ZnO are known from 1935, whereas detailed values of optical parameters were available in mid 50s. Systematic investigations of ZnO as a compound semiconductor were performed in 1960.

Currently, research on ZnO as a semiconducting material sees a renaissance after intensive research periods in the 1950s and 1970s. Even though good quality, thin films (by chemical vapor deposition) were prepared in 1970, only recently ZnO attracts an increasing attention. Since about 1990, an increase of the number of publications on ZnO occurred, and more recent reviews on ZnO have been published [39].

Zinc oxide is an inorganic compound with ZnO formula. Where, commonly appears as a white powder, almost insoluble in water. The powder is widely used as an additive into many materials such as ceramics, glass, cement, rubber (car tyres), lubricants, paints ointments, adhesives, sealants, pigments, foods (source of Zn nutrient), batteries, fire retardants, etc. ZnO is presented in the Earth crust as a mineral zincite; however, most ZnO used commercially is produced synthetically [26].

I.5.1 Properties of Zinc Oxide:

I.5.1.1 Structural Properties:

Zinc oxide is a wide-bandgap II-VI compound semiconductor, it can crystallize in three crystallographic phases as shown in Figure I-8, according to the conditions of elaboration: the cubic rocksalt structure (NaCl), the hexagonal Wurtzite structure and the structure zinc blend. Mostly, the group II–VI binary compound semiconductors have either cubic zinc blend or hexagonal wurtzite structure.

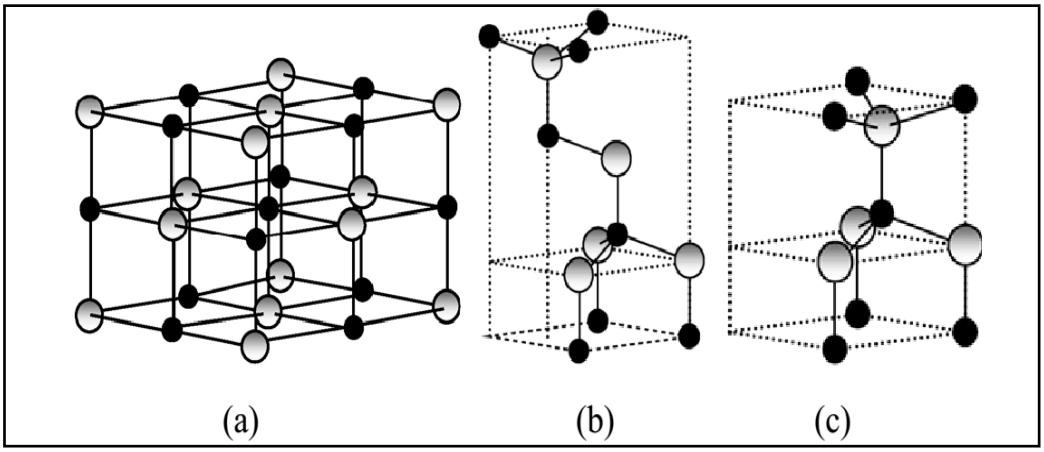

Figure I-8: ZnO crystal structures: (a) Cubic rocksalt, (b) Cubic zinc blend, (c) Hexagonal wurtzite (Zinc atoms in gray and oxygen in black) [34].

The Blend structure is obtained when ZnO is deposited on certain substrates of cubic symmetry, the rocksalt structure is observed under very high pressures [$\sim 10\ GPa$], the thermodynamically stable structure at room temperature is the hexagonal wurtzite structure with the lattice parameters a $=$ b $=$ 3.24982 Å ; c $=$ 5.20661 Å [16].

The hexagonal lattice is characterized by two interconnecting sub lattices of $Zn^{2+}$and O^{2-}in such a way that each Zn^{2+} ion is surrounded by a tetrahedron of O^{2-} ions, and vice-versa. The tetrahedral coordination in ZnO results in non-central symmetric structure [14], but displaced by 0.11 Å in a direction parallel to the c axis [34], which subsequently results in strong piezoelectric, pyroelectric effects, and spontaneous polarization, that is also a key factor in crystal growth, etching, and defect generation [14].

In the hexagonal wurtzite structure, it has a polar hexagonal axis, the c-axis, chosen to be parallel to Z (0001).The zinc atoms locate almost in the position of hexagonal close packing, as shown in following Figure I-9, Table I-1 illustrates some properties of the Wurtzite structure of ZnO.

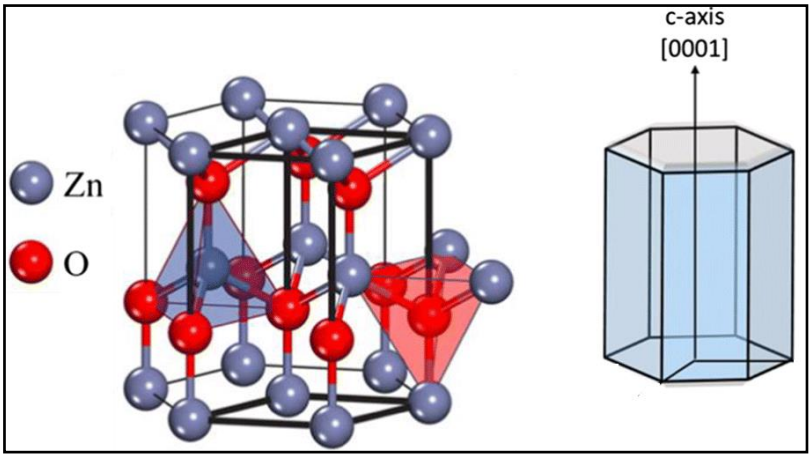

Figure I-9: Wurtzite crystal structure of ZnO with hexagonal unit cell [40].

Table I-1: Physical properties of the zinc oxide in the wurtzite form [16, 34, 39, 41]

Properties	**Parameters (Value) at 300 K**
Crystalline structure	**Wurtzite**
Lattice parameters	$\mathbf{a_0 = b_0 = 3.249}$ Å
	$\mathbf{c_0 = 5.206}$ Å
	$\frac{\mathbf{c_0}}{\mathbf{a_0}} = \mathbf{1,602\ (1,633\ in\ an\ ideal\ wurtzite\ structure)}$
Refractive index	$\mathbf{2.008 - 2.029}$
Band gap energy	$\mathbf{3.37\ eV, direct}$
Melting point	$\mathbf{1975}$ ℃
Density $(\mathbf{g/cm^3})$	$\mathbf{5.606}$
Electron effective mass	$\mathbf{0.28\ m_0}$
Exciton binding energy	**60 meV**

I.5.1.2 Optical properties and luminescence:

Zinc oxide is a material transparent in visible with high transmittance (T > 80%). The refractive index n of bulk ZnO is equal to two. In thin films, the value of the index n and the absorption coefficient is dependent on the conditions of thin layers' elaboration, where n has a value between 1.7 and 2.2. ZnO has the extremely large exciton binding energy of (60 meV), which is much greater than the thermal energy (26 meV) at room temperature [26].

For the use of zinc oxide in various applications, several authors have studied its various optical properties such as transmission, absorption, reflection, geometry [14], optical gap, and photoluminescence. The research results show that its optical property is related to several parameters that we quote the thickness, the optical gap, the surface roughness, the doping, the crystalline quality of the film, and the deposition method [16].

The photoluminescence of ZnO typically consists of UV emission $(350\ \text{nm})$, and broad visible band emission $(550\ \text{nm})$. The UV emission observed in ZnO is believed to result from band edge exciton emission while the visible emission is due to defect emission. Green emission is the most commonly observed visible emission in ZnO, although other colors like yellow and orange have also been reported. The origin of the green emission is the most controversial. It was suggested that the green emission was due to transitions between electron close to the conduction band and a deeply trapped hole [26].

I.5.1.3 Electrical and electronic properties:

The electronic structure of the zinc and oxygen is:

$$O:\ 1s^2 2s^2 2p^4$$

$$Zn:\ 1s^2 2s^2 2p^6 3s^2 3p^6 3d^{10} 4s^2$$

Production of quality p-type ZnO films has been problematic, mostly due to defects caused by dopants induced stresses in the crystal. Very low formation energies for oxygen vacancies and zinc interstitials in ZnO have been calculated and likely explain the native n-type conductivity observed in as-grown films [26].

The electrical properties of ZnO thin films, such as: electrical resistivity, charge carrier concentration, and mobility are determined by Hall Effect measurements. The electrical resistivity (ρ) of an n-type thin film depends on the electron density (n) in the conduction band and their mobility (μ), where e is the electron charge. It is known that e is a constant [16]:

$$\sigma = \frac{1}{\rho} = en\mu_n \quad \text{(I.1)}$$

The literature [42] indicates, “If an oxygen vacancy is created in a perfect crystal, two electrons are created in the crystal and contributed as ionized donors”. But, if there is too much oxygen created in the thin films, sub-oxides will form, causing the resistivity to rise.” In addition to the oxygen vacancies, doping (most used dopants are Al, Ga, In, B, Si, Ge, F) also can change the electrical conductivity of ZnO. As host cations are substituted by elements with a valence higher than that of the host, the extra electrons can become conduction electrons. To avoid the

charge neutrality, substitution of a higher valence element creates extra electrons. It is well known that pure zinc oxide films usually have a characteristic high resistivity due to their low carrier concentration. Therefore, in order to decrease resistivity, we can increase either the carrier concentration or the carrier mobility in zinc oxide thin films. The former is probably obtained by oxygen and/or zinc non-stoichiometry, or doping with an impurity [26].

Table I-2: Some electrical properties of ZnO [16].

Properties	**Values**
Nature of the band gap	**Direct**
The band gap at 300 °K (eV)	$\mathbf{3.34 \pm 0.02}$
Conductivity type	$\boldsymbol{n\ and\ (p)}$
Electrical conductivity ($(\Omega.\mathbf{cm})^{-1}$)	$\mathbf{10^{-6} - 10^{2}}$
Charge carrier density ($\mathbf{cm^{-3}}$)	$\mathbf{10^{15} - 10^{21}}$
Density of states in CB ($\mathbf{cm^{-3}}$)	$\mathbf{3.71 \times 10^{18}}$
Density of states in VB ($\mathbf{cm^{-3}}$)	$\mathbf{1.16 \times 10^{19}}$
Electrons mobility ($\mathbf{cm^2/V.s}$)	$\mathbf{0.2 - 200}$
Holes mobility ($\mathbf{cm^2/V.s}$)	$\mathbf{5 - 50}$
The effective mass of electrons	$\mathbf{0.28\ m_0}$
The effective mass of holes	$\mathbf{0.60\ m_0}$
Thermal velocity of electrons ($\mathbf{cm.s^{-1}}$)	$\mathbf{2.2 \times 10^{7}}$
Thermal velocity of holes ($\mathbf{cm.s^{-1}}$)	$\mathbf{1.5 \times 10^{7}}$
Relative dielectric constant $\varepsilon_r = \frac{\varepsilon}{\varepsilon_0} t$	$\boldsymbol{\varepsilon_{//} = 8.7 / \varepsilon_{\perp} = 7.8}$

I.5.1.4 Review of doped zinc oxide thin films:

Many types of dopants have been advantageously used (Al, In, As, Ga, B, S, Sn, Mn, etc.) for many important applications in ZnO thin films; these dopant elements offer a manner to regulate the electrical, optical, and magnetic properties. They make doped ZnO films promising candidates as conductors with high transparency in the visible light range and high conductivity.

Even though the standard transparent conductors in industry are ITO and FTO, there is huge interest in finding more stable and cheaper alternatives [14].

The main problem for the application of ZnO as a material for electro-optic devices is a bipolar doping. This problem is found frequently for wide band gap materials, namely that doping of one type (n-type) is easily possible up to high densities, while the opposite type (p-type) is hardly achievable. The semiconductors ZnO is generally n-type [39].

I.5.2 Zinc oxide applications:

Zinc oxide is such a former technological material. Already in the Bronze Age, it was produced as a byproduct of copper ore smelting, used for healing of wounds. Early in history, it was also used for the production of brass (Cu-Zn alloy). This was the major application of ZnO for many centuries before metallic zinc replaced the oxide. With the start of the industrial age in the middle of the nineteenth century, ZnO was used in white paints (Chinese white), in rubber for the activation of the vulcanization process, and in porcelain enamels [43].

Research interest in ZnO is enormously growing because of its excellent optical, electrical, magnetic, piezoelectric, catalytic, and gas-sensing properties that made it specifically attractive for nano-electronic, optoelectronic, nano-photonic, and piezoelectric devices. Different nano-structures of ZnO, including; nano-rods, nano-wires, nano-tubes, and nano-ribbons [44].

Zinc Oxide also has antibacterial and deodorizing properties. For this reason, it is employed in medical applications such as in baby powder and creams to treat conditions, such as diaper rash, other skin irritations, and even dandruff. Due to its reflective properties, it is also used in sun blocks and can often be seen on the nose and lips of lifeguards at the beach [14].

REFERENCES

[1] Y. Aoun, B. Benhaoua, S. Benramache, B. Gasmi. Effect of annealing temperature on structural, optical and electrical properties of zinc oxide (ZnO) thin films deposited by spray pyrolysis technique, Optik, 126 (24) :5407-5411, (2015).

[2] Mattox DM, Handbook of physical vapor deposition (PVD) processing, William Andrew (2010).

[3] K. Wasa, M. Kitabatake, H. Adachi, Thin film materials technology: sputtering of control compound materials, Springer Science & Business Media. (2004)

[4] K. Seshan, Handbook of Thin-film Deposition Processes and Techniques: Principles Methods Equipment and Applications, Noyes Publications/William Andrew Pub (2002).

[5] K. Wasa, M. Kitabatake, H. Adachi, K. Wasa, M. Kitabatake, H. Adachi, Thin Film Processes, In: Thin Film Materials Technology, Norwich, NY: William Andrew Publishing, 17–69; (2004).

[6] Y. Benkhetta, Elaboration and characterization of thin layers of zinc oxide (ZnO) deposited by ultrasonic spray for photovoltaic and optoelectronic. Doctoral Thesis, University of Biskra, Algeria (2019).

[7] R. Messemche, Elaboration and characterization of undoped and doped titanium dioxide thin layers by sol gel (spin coating) for photocatalytic applications. Doctoral Thesis, University of Biskra, Algeria (2021).

[8] J. A. Venables, Introduction to Surface and Thin Film Processes; Cambridge University Press, (2000).

[9] A. Pimpinelli, Villain, J. Physics of Crystal Growth; Cambridge University Press, (1999)

[10] L. B. Freund, S. Suresh, Thin Film Materials: Stress, Defect Formation and Surface Evolution; Cambridge University Press, (2003).

[11] K. J. M. Bishop, C. E. Wilmer, S. Soh, B. A. Grzybowski, Nanoscale Forces and Their Uses in Self-assembly. Small, 5, 1600–30, (2009).

[12] S. Brochen, electrical properties of ZnO single crystale, doctoral thesis, Grenoble University (2006).

[13] High-resolution characterization of TiN diffusion barrier layers - Scientific Figure on Research Gate (2022).

[14] M. Othmane, Synthesis and characterization of Zinc Oxide (ZnO) Thin films deposited by spray pyrolysis for applying: electronics and photonics. Doctoral Thesis, University of Biskra, Algeria (2018).

[15] Overview Metallization Technology, Physical Vapor Deposition PVD (2015).

[16] N. Abdelouahab, Preparation and characterization of thin films nanostructures based on ZnO and other oxides. Doctoral Thesis, University of Oum El Bouaghi, Algeria (2019).

[17] O. Olayinka. Abegunde, E. Titilayo Akinlabi, O. Philip Oladijo, S. Akinlabi, A. UchennaUde, Overview of thin film deposition techniques, AIMS Materials Science, 6(2), 174-199, (2019).

[18] DM. Mattox, Atomistic Film Growth and Some Growth-Related Film Properties, Handbook of Physical Vapor Deposition (PVD) Processing (1998).

[19] U. Seyfert, U. Heisig, G. Teschner, et al. 40 Years of Industrial Magnetron Sputtering in Europe. SVC Bulletin Fall, 22–26, (2015).

[20] K. Seshan, Handbook of thin-film deposition processes and Techniques, Principles, Methods, Equipment and Applications, Noyes Publications/William Andrew Publishing (2001).

[21] V. Teixeira, H. Cui, L. Meng, et al. Amorphous ITO thin films prepared by DC sputtering for electrochromic applications. Thin Solid Films, 420: 70–75, (2002).

[22] K. Utsumi, H. Iigusa, R. Tokumaru, et al. Study on In_2O_3–SnO_2 transparent and conductive films prepared by d.c. sputtering using high density ceramic targets. Thin Solid Films, 445: 229–234, (2003).

[23] Cash Jr JH, Cunningham JA Rf sputtering method. U.S. Patent, 3,677,924, (1972).

[24] T. You, O. Niwa, M. Tomita, et al. Characterization and electrochemical properties of highly dispersed copper oxide/hydroxide nanoparticles in graphite-like carbon films prepared by RF sputtering method. Electrochem Commun, 4: 468–471, (2002).

[25] A. Mennad, Les techniques de dépôt de couches minces et leurs applications, Revue des Energies Renouvelables, vol. 18, pp. 713–719 (2015).

[26] M. Dahnoun, Preparation and characterization of Titanium dioxide and Zinc oxide thin films via Sol-Gel (spin coating) technique for optoelectronic applications. Doctoral Thesis, University of Biskra, Algeria (2019).

[27] M. Raileanu, Sol-gel method under visning materials, pp 37, (2006).

[28] E. Yilmaz, M. Soylak, Functionalized nanomaterials for sample preparation methods, Chaudhery Mustansar Hussain, Handbook of Nanomaterials in Analytical Chemistry, Elsevier, ,375-413, (2020).

[29] J. Puetz, M.A. Aegerter, Sol-gel technologies for glass producers and users; Dip coating technique, (2004).

[30] K. Kakaei, M. D. Esrafili, A. Ehsani, Ch.8, Graphene and Anticorrosive Properties, Interface Science and Technology, Elsevier, V.27,303-337, (2019).

[31] C.J. Brinker, A.J. Hurd, G.C. Frye, P.R. Schunk, C.S. Ashley, Sol-gel thin film formation, J. Ceram. Soc. Jpn. 99 (1991) 862–877.

[32] A. Yahia, Optimization of indium oxide thin films properties prepared by sol gel spin coating process for optoelectronic applications, Doctoral Thesis, University of Biskra, Algeria (2020).

[33] B. S. Yilbas, Abd Al-Sharafi, H. Ali, Chapter 3 - Surfaces for Self-Cleaning, Self-Cleaning of Surfaces and Water Droplet Mobility, Elsevier, (2019), 45-98.

[34] Saâd rahmane, Elaboration et caractérisation de couches minces par spray pyrolyse et pulvérisation magnétron, Doctoral Thesis, University of Biskra, Algeria (2008).

[35] A. Mallick, D. Basak, Revisiting the electrical and optical transmission properties of co-doped ZnO thin films as n-type TCOs, Progress in Materials Science, Vol 96, (2018), P 86-110.

[36] King Phil & Veal Tim, Conductivity in transparent oxide semiconductors, Journal of physics Condensed matter: An Institute of Physics journal, 23 (2011).

[37] G. Haacke, New figure of merit for transparent conductors, Journal of Applied Physics 47, 4086 (1976).

[38] A. Allag, Optimisation des conditions d'élaboration des couches minces d'oxyde d'étain SnO_2 par spray. Doctoral Thesis, University of Biskra, Algeria (2018).

[39] F. BOUAICHI, Deposition and analysis of Zinc Oxide thin films elaborated using spray pyrolysis for photovoltaic applications. Doctoral Thesis, University of Biskra, Algeria (2019).

[40] M. Samadi, M. Zirak, A. Naseri, Design and tailoring of one-dimensional ZnO nanomaterials for photocatalytic degradation of organic dyes: a review Res. Chem. Intermed 45, 2197–2254 (2019).

[41] C. Nadia, Traitement de l'oxyde de zinc et étude de ses propriétés physicochimiques superficielles, doctoral thesis, Badji Mokhtar Annaba University, Algeria (2014).

[42] R. Eason, Pulsed Laser Deposition of Thin Films, Wiley Interscience, New York, USA, (2007).

[43] E. Klaus, A. Klein, B. Rech, Transparent conductive zinc oxide: basics and applications in thin film solar cells. Springer-Verlag, Berlin Heidelberg, (2008).

[44] Vyas Sumit, Johnson Matthey Technology Review, Vol 64, (2020), pp. 202-218 (17).

Chapter II:

Elaboration technique and Characterization tools.

II.1 Introduction:

Dip-coating is a simple method that provides a thin film with good quality using sol- gel process. The properties and the component of thin film obtained can be tailored by controlling the deposition parameters and the solution's component.

This chapter is presenting the elaboration technique and characterization tools of thin films obtained by sol-gel method. Moreover, detailed information about sol-gel process and its steps plus the chemical reactions requires to form a thin film.

II.2 Sol-gel Method:

Referring back to the first chapter, ZnO thin films can be deposited using different techniques, as: PVD, CVD, Laser ablation, Spray pyrolysis, and so on. Among these methods, sol-gel method interestingly offers a cheap and easy method with a high throughput. In this method (which is also called soft chemistry), a solid material is also formed from a solution by using a sol or a gel as an intermediate step [1]. The basic idea of the sol-gel process is simple, a mixture of liquid precursors is converted to a solid by chemical reactions of polymerization type at low temperature [2]. With this technique, the transformation of chemical precursors into an oxide network requires hydrolysis and condensation reactions [2,3].

II.2.1 Sol-gel process steps:

II.2.1.1 Hydrolysis:

The synthesis of metal oxides by dissolving metal alkoxides in organic solvents is one group of sol-gel methods. This method is mainly based on the poly-condensation of metal-alkoxides $\mathbf{M(OR)_n.R}$ is usually an alkyl group and **n** is the oxidation level of the metal. The synthesis involves two steps: The first step is hydrolysis in which reactive **M-OH** groups are formed by the following reaction (II-1) [1]:

$$M - OR + H_2O \Rightarrow \ M - OH + ROH \qquad \text{(II-1)}$$

II.2.1.2 Condensation:

Condensation is liberating small molecules, such as: water and alcohol. The reaction can be expressed as (II-2) [1]:

$$M - OH + RO - M \Rightarrow \ M - OH - M + ROH \qquad \text{(II-2)}$$

The process of formation of ZnO films using zinc acetate precursor is illustrated below which proceeds via the process of hydrolysis, condensation, and poly-condensation. The reaction is illustrated as follows (II-3) [4]:

$$Zn(OH)(CH_3COO)_2 + OH^- \Rightarrow \ Zn(OH)_2 + CH_3COO^- \qquad \text{(II-3)}$$

If two molecules of $\mathbf{Zn(OH)_2}$condense, the reaction can be expressed as (II-4):

$$HO - Zn - OH + HO - Zn - OH \Rightarrow \ HO - Zn - O - Zn - OH + H_2O \qquad \text{(II-4)}$$

The process would continue. After the evaporation of the water molecules, this would result in a final product which can be written as $\mathbf{HO - (Zn - O - Zn)_n - OH}$ where **n** is the number of molecules taking part in the condensation process (poly-condensation) [4].

II.2.1.3 Gelation:

The reactions cause gelation and formation a gel up of **M-O-M** (or **M-OH-M**) chains, which increases viscosity by time. This gel contains unreacted solvent and precursors. The solid phase is typically a condensed polymeric sol where the particles have entangled to form a three-dimensional network. The time taken for « sol » to transform to a « gel » defined as the gelation point or the gelation time [5].

II.2.1.4 Ageing:

The continuing chemical and physical changes during ageing after gelation are significant. During this process, further cross-links continuous, the gel shrinks as the covalent links replace non-bonded contacts and the pore sizes, and pore wall strengths change with the evolution of the gel's structure [6].

II.2.1.5 Drying:

The gel has a high ratio of water and three-dimensional interconnected pores inside the structure. Before the pore is closed during the densification process, drying is needed to remove the liquid trapped in the interconnected pores. On the other hand, removal of the liquid from the tiny pores causes significant stress resulting from inhomogeneous shrinkage. Therefore, the main problem that had to be overcome is cracking due to the large stress in the structure. For small cross sections, such as: powder, coating, or fiber, the drying stress is small and can be accommodated by the materials, so there is not a special care required to avoid cracking for those sol-gel structures. While for monolithic objects greater than 1 cm, drying stress developed in

ambient atmosphere can introduce catastrophic cracking, as a result the control of the chemistry of each processing step is essential to prevent cracking during drying [6].

II.2.1.6 Densification:

Heat treatment of the porous gel at high temperature is necessary for the production of dense glass or ceramics from a gel. After the high temperature annealing, the pores are eliminated, and the density of the sol-gel materials ultimately becomes equivalent to that of the fused glass. The densification temperature depends considerably on the pore's dimension, the degree of connection of the pores, and the surface areas in the structure [6].

Solutions usually contain precursors, solvents, stabilizers, and water; these contents of which control the properties of the sol-gel. Therefore, the deposited ZnO films are affected by each, so the selection of each component must be very careful and precise.

II.2.2 Precursor:

In general, the most used precursors in sol-gel process are: inorganic (salts) and metallo-organic (like alkoxide, acetate...). In aqueous or organic solvents, the precursors are hydrolyzed and condensed to form inorganic polymers composed of **M-O-M** bonds [2,7].

Several zinc precursors have been used: nitrate, chloride, perchlorate, acetylacetonate, and alkoxides, such as: ethoxide and propoxide; however, the most often used is the acetate dehydrate [8].

Isaias Limón-Rochab reported in [9] that Zinc oxide nanoparticles using zinc nitrate and zinc acetate as precursors were successfully synthesized following the sol–gel method. The morphology, crystalline structure, and physicochemical properties depend on the zinc oxide precursor [9].

II.2.3 Solvents:

The solvent must present a relatively high dielectric constant in order to dissolve the inorganic and organic salts [8]. It is well known that the dielectric constant is dependent on chain length [1]. Among the various solvents, alcohols with low number of carbon atoms (maximum four) are the most widely used solvents. Methanol, ethanol, 1-propanol, 2-propanol, 1-butanol, and 2-methoxyethanol are some of the solvents used more compared to the others [1].

In addition, a few works use ethylene glycol ($HOCH_2CH_2OH$) as a solvent that has a dielectric constant of 40.61 (at 25°C) and a boiling point of 197.4°C [8].

Table II-1: Dielectric constants and boiling points for some alcohols [8].

Alcohol	Formula	Dielectric constant at 20 °C	Boiling point (°C)
Methanol	CH_3OH	**32.35**	**64.7**
Ethanol	CH_3CH_2OH	**25.00**	**78.3**
1-Propanol	$CH_3CH_2CH_2OH$	**20.81**	**97.2**
2-Propanol	$CH_3CH(OH)CH_3$	**18.62**	**82.2**
1-Butanol	$CH_3CH_2CH_2CH_2OH$	**17.80**	**117.7**
2-Butanol	$CH_3CH_2CH(OH)CH_3$	**15.80**	**99.5**
2-Methoxyethanol	$CH_3OCH_2CH_2OH$	**16.90**	**124.6**

The use of solvents with higher boiling points, like 2-methoxyethanol and MEA (monoethanolamine), resulted in strongly preferential orientation of ZnO crystals as demonstrated by Ohyama et al. [10]. These authors suggested, as an explanation of the effect of the solvent boiling point for ZnO crystallization, that a solvent of higher boiling point would evaporate more slowly on heating, allowing the structural relaxation of the gel film before crystallization [8].

II.2.4 Stabilizers:

Stabilizers are chemical species containing at least one functional group. Alkali metal hydroxide, carboxylic acid, alkanolamines, alkylamines, acetylacetone, and polyalcohols are some of the stabilizers used for depositing ZnO nanostructures. There are several reasons for their usage: in some cases, they contribute to the dissolving of zinc salt in the alcoholic solvents [1]. For instance, Zinc acetate dehydrate (ZAD) has a limited solubility in alcohols like ethanol and 2-propanol in the absence of other agents or heating [8]. The agents as (mono- to tri-) ethanolamine or lactic acid help in the accomplishment of dissolution and the stable sol's formation [11]. Another role of stabilizers is stabilizing ligands, preventing the rapid precipitation of zinc hydroxide, and hence contributing to the formation of stable sols [1].

II.2.5 Advantage and disadvantage of sol-gel:

This method has the advantage of being simple to implement because of the needless of heavy equipment, and it is also easy to change the various component's quantities of the film (Zn, O, Al…) using precursor dose. Otherwise, the final stoichiometry of the film is quite difficult to obtain. It has the advantage of being suitable for substrates with complex shapes. On the contrary,

the main disadvantage of this technique is the low thickness of the deposit film which is about (50 nm) after one pass of the process [2].

II.3 The used technique dip-coating:

ZnO thin films can be elaborated by dip-coating technique using sol-gel method which can be applied to all types of precursors solutions. It should be noted that this seemingly simple formation process of film via dip-coating involves complex chemical and physical multi-variable parameters. During dipping and coating, the thickness and morphology of depositing thin films were determined by several parameters, such as: immersion time, withdrawal speed, dip-coating cycles, density and viscosity, surface tension, substrate surface, and evaporation conditions of coating solutions, etc [12].

In this technique, the substrate is withdrawn vertically from the coating bath at a constant speed U_0 (Figure II-1) [13]. The moving substrate entrains the liquid in a viscous boundary layer that split in two at the free surface (point **S** in figure II-1) returning the outer layer to the bath [14]. Since the solvent is evaporating and draining, the entrained film acquires an approximate wedge shape that terminates in a well-defined drying line (x=0) (figure II-2) [13]. When the upward moving flux is balanced due to the evaporation, the film position and shape of the film profile remain steady with respect to the coating bath surface. Within the thinning film, the inorganic species are progressively concentrated by evaporation, leading to aggregation, gelation, and final drying to form a type of a dry gel or xerogel. Figure II-2 indicates schematically the microscopic processes which occur within the thinning film [14].

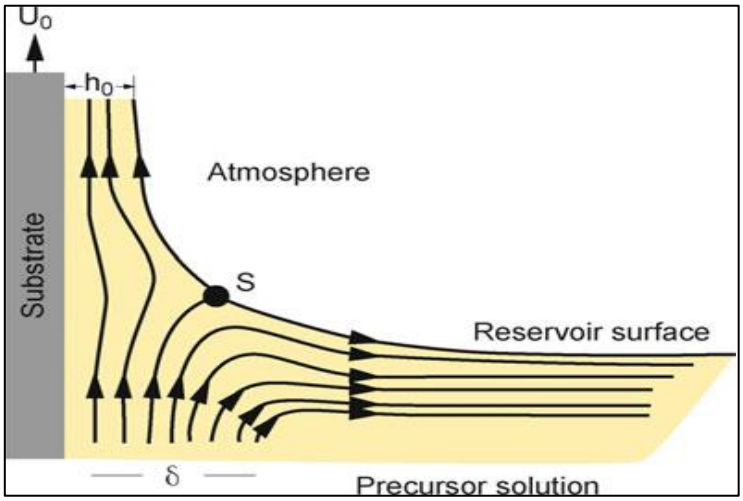

Figure II-1: Detail of the flow patterns (streamlines) during the dip-coating process. U_0 is the withdrawal speed, S is the stagnation point, δ the boundary layer, and h_0 is the thickness of the entrained fluid film on the substrate [7].

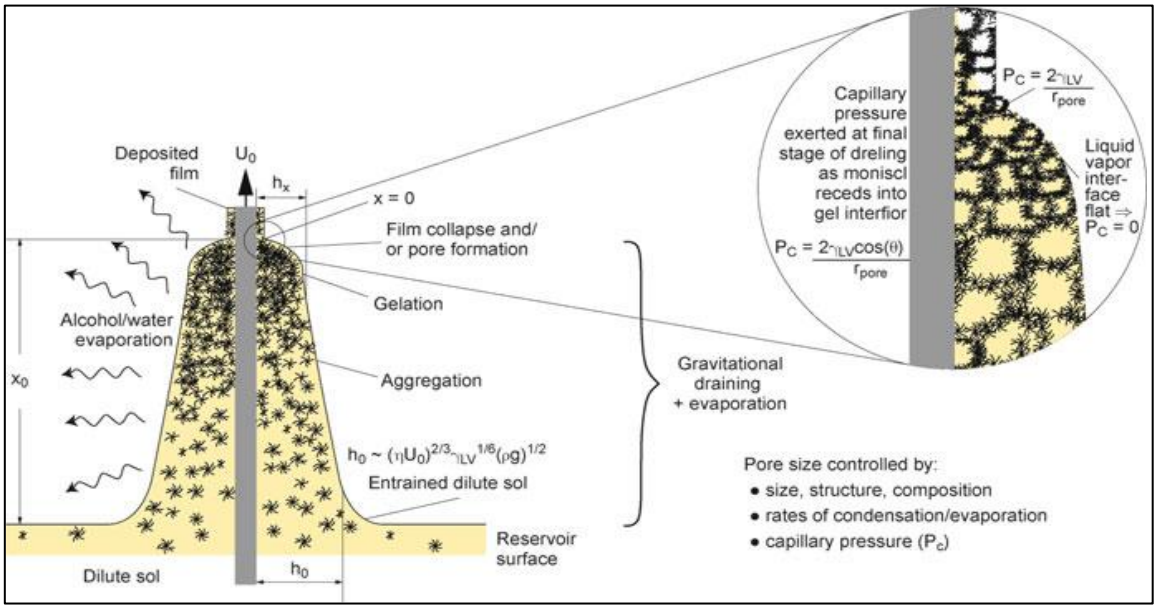

Figure II-2: Schematic of the steady-state dip-coating process, showing the sequential stages of structural development that result from draining accompanied by solvent evaporation and continued condensation reactions. U_0 is the withdrawal speed [7].

The thickness is tuned not only through the adjustment of the withdrawal speed but also by the concentration of the solution, knowing that increasing the speed or the solution concentration, or both, leads to thicker films. In most cases, the deposition is performed with solutions loaded with around 5 to 10% in weight of the nonvolatile species and at speeds ranging from 1 to 10 mms^{-1}. The thickness typically is between 50 and 500 nm. Appropriate solvents are alcohols because of low surface tension, and they are fairly volatile to promote relatively fast evaporation. Both properties are necessary to obtain highly homogeneous films. As mentioned in the beginning of this chapter, that in sol-gel process, the basic chemistry involves hydrolysis of the inorganic molecular precursor and polycondensation into extended solids. The first reaction needs to be initiated for the second one to start. The two reactions start thus in the solution, run during deposition along the evaporation process, and they are generally completed on the dry film during a final thermal treatment [14].

II.3.1 Advantage and disadvantage of dip-coating:

Some advantages of dip-coating over other methods:

- Dip-coating is a facile and economical technique widely used in many industrial fields to deposit onto any substrate [12].
- Can coats different shapes and natures of samples [12].
- It provides a full coverage of the substrate.

The disadvantages include the following:

- Coats two sides of the substrate can cause complications if only on side needs coating [15].
- Sensitive to the atmosphere.
- The limitation of thickness.
- It is a time consuming method.
- Poor uniformity of surface of the thin film.
- A comparatively large amount of solution is required, especially for large substrates. This is particularly inconvenient if the solution is expensive or unstable [15].

II.4 Characterization tools of thin films:

II.4.1 Thickness measurement:

The thickness is an essential property of a thin film that defines its physical characteristics. Various methods including profilometer, SEM, the gravimetric method, and Swanepoel method have been utilized to measure the film thickness.

II.4.1.1 Stylus profilometry:

This is a technique consisting of scanning a sample between two fixed points using a diamond stylus. The film thickness could be measured by forming a step between the film surface and the uncovered substrate surface. This transition allows us to acquire the profile of the sample in the considered vertical plane [2].

The uncovered surface can be produced by masking portions of the substrate during deposition, or by removing parts of the film after deposition [16].

II.4.1.2 The gravimetric method:

This method consists in measuring the change in weight of the substrate due to film deposition. The thickness **d** of the film can be calculated using this equation (II-5) [17,18]:

$$d = \frac{\Delta m}{A.\rho} \qquad \text{(II-5)}$$

- Δm: Is the weight difference (expressed in gramme).
- A: Is the area of the film.
- ρ: Is the density of material.

II.4.1.3 The scanning electronic microscope (SEM)

SEM allows us to obtain the thickness measurement with a precision about 5 nm, for the films whose thickness is more than 100 nm. On the other hand, if the film is extremely thin, it is difficult to accurately estimate the thickness of the film, because of the difficulties of visualization at high magnifications [2]. An example of thickness measurement is shown in Figure II-3 from [2]:

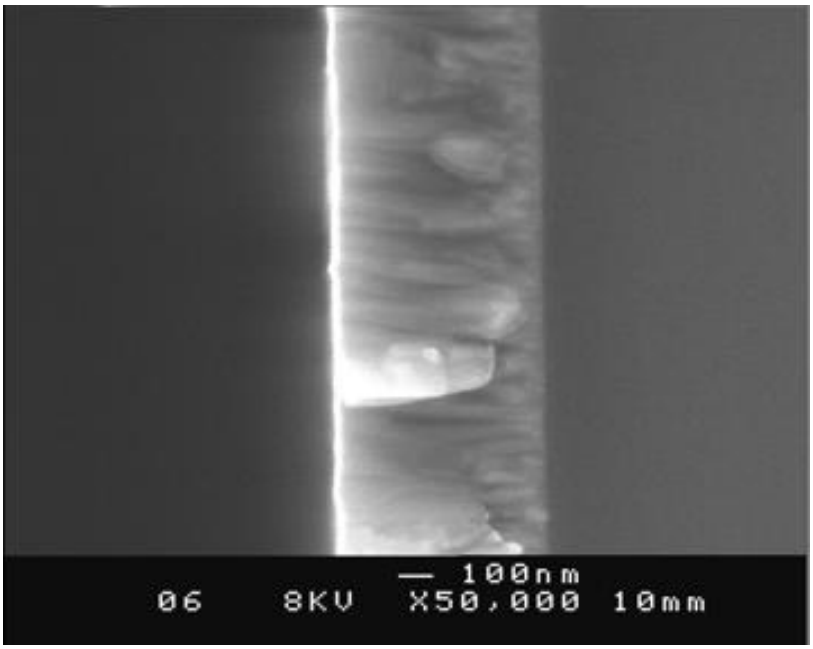

Figure II-3: SEM image of ZnO:Al thin, shows that the thickness is about 600 nm [2].

II.4.1.4 Swanepoel method:

Swanepoel's method can be used to determine the thickness of the film from a transmission spectrum obtained in UV-Vis domain if it presents interference fringes, by the basic equation given below (II-6) [2,19]:

$$d = \frac{\lambda_1 \lambda_2}{2(\lambda_1 n_2 - \lambda_2 n_1)} \quad \text{(II-6)}$$

Where n_1 and n_2 are the refractive index of the film for the wavelength λ_1 and λ_2 respectively.

The refractive index can be calculated with the following relation (II-7):

$$n = \{N + (N^2 - S^2)^{0.5}\}^{0.5} \quad \text{(II-7)}$$

With:
$$N = 2S \times [(T_M - T_m)/ T_M T_m)] + (S^2 + 1)/2 \quad \text{(II-8)}$$

Where S is the refractive index of the substrate which is equal 1.5 for the glass.

T_M and T_m are the maximum and minimum transmittance respectively correspond with the wavelength λ [2,19].

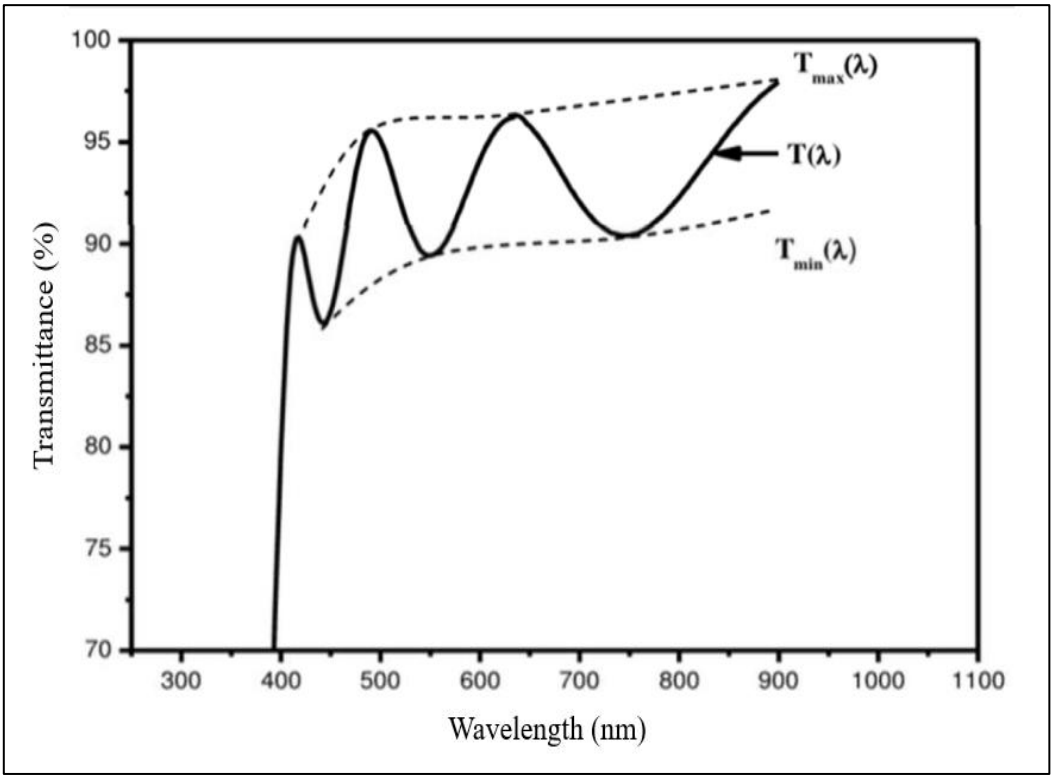

Figure II-4: Example of experimental transmittance Where T_{max} and T_{min} are the maximum and minimum of the envelopes [20].

II.4.2 Structural characterization with X-Ray diffraction:

X-ray diffraction is a characterization used to find out the nature of the materials as crystalline or amorphous. It provides a detailed information on structure, such as: phases (the peak position), crystallite size, and crystal orientation [2,21]. XRD peaks are produced by constructive interference of monochromatic X-rays and a crystalline sample, where the X-rays incident with an angleθ on a crystal surface and reflected from it with a diffracted angle 2θ (Figure II-5).

The most significant advantage of this technique is that it is non destructive, as well as being faster and requiring a quite small sample. Also, it can be conducted at room temperature and pressure [22].

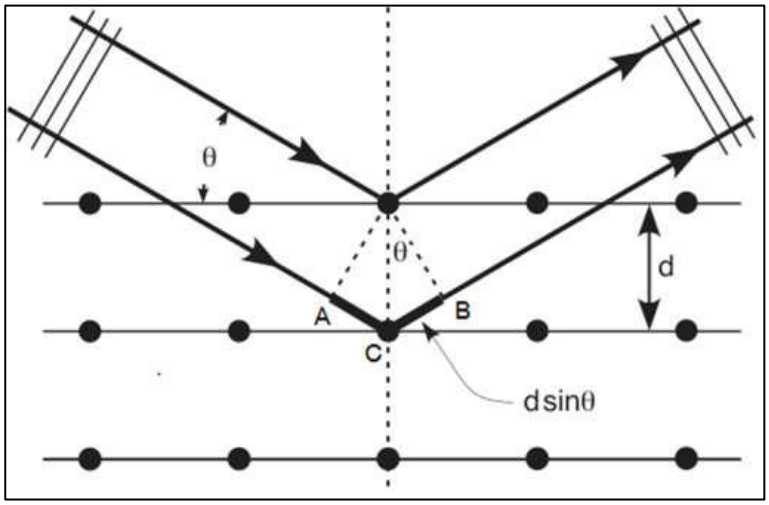

Figure II-5: Reflection of X-rays from two planes of atoms in a solid [2].

The reflection follows Bragg's law (II-9) [2]:

$$2.d_{hkl}.\sin\theta = n.\lambda \qquad \text{(II-9)}$$

Where d is the spacing between diffracting planes, θ is the incident angle, λ is the wavelength of the X-rays, and n is a positive integer. In order to identify the existence of different crystallographic phases in the film, their relative abundance, the lattice parameters, and any preferred orientations, experimentally obtained diffraction patterns of the sample must be compared to JCPDS data cards (Figure II-6).

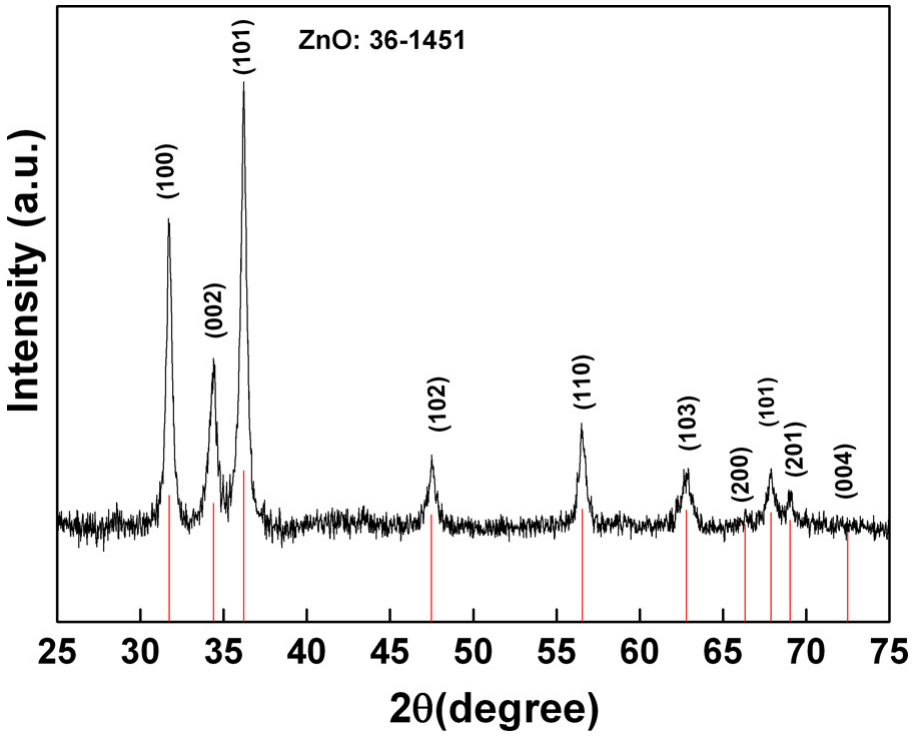

Figure II-6: X-Ray diffraction (XRD) spectra of ZnO powder stoichiometric (JCPDS 36-1451) [23].

II.4.2.1 Determination of the interreticular distances and the cell parameters:

Using the (hkl) parameters and the interplanar spacing d, the lattice parameter values for wurtzite structure (ZnO structure) can be determined using the formula below (II-10) [2]:

$$\frac{1}{d_{hkl}^2} = \frac{4}{3}\left(\frac{h^2 + hk + k^2}{a^2}\right) + \frac{l^2}{c^2} \qquad \text{(II-10)}$$

In (002) peak we determine the parameter c:

$$c = d_{hkl} \times l \qquad \text{(II-11)}$$

Using Bragg's law (II-9) in (100) peak we determine the parameter a [20]:

$$a = \frac{\lambda}{\sqrt{3} \times sin\theta_{100}} \qquad \text{(II-12)}$$

II.4.2.2 Determination of the crystallite size:

The crystallite size of the thin film can be estimated from the width of the diffraction peak, using Debye Scherrer's formula (II-13) [24,25], it is notable that the increase in intensity of the diffraction peak and also the narrowing of the peak, i.e., decrease in the full width at half maximum (FWHM) of the peak, with the increase in thickness indicate the crystallinity improvement of the films [26].

$$D = \frac{K.\lambda}{\beta.\cos\theta}[nm] \qquad \text{(II-13)}$$

Where K is a constant known as shape factor and taken as 0.94, λ is the wavelength of X-rays, β is the full-width at half maximum (FWHM), and θ is Bragg angle (θ and β in radians).

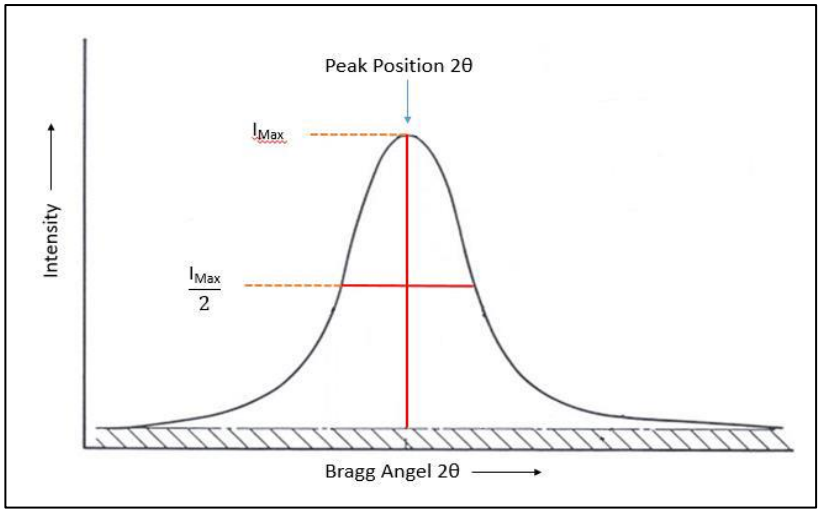

Figure II-7: FWHM of XRD peak, where $\frac{I_{Max}}{2}$ is the full-width at half maximum (β) [27].

II.4.2.3 Determination of strain:

Strain (ε) of the thin films is estimated using the equation (II-14) [28]:

$$\varepsilon = \frac{\beta . \cos\theta}{4} \qquad \text{(II-14)}$$

II.4.3 Morphological characterization

II.4.3.1 Scanning electron microscope:

SEM is a scanning electron microscope provides a detailed information of the sample including its morphology, topography, composition, and crystallographic information. Thus, SEM is a multipurpose instrument which is able to examine and analyze the materials with high resolution [29].

The SEM instrument is based on the principle that the primary electrons beam released from the source with a few keV accelerating voltage [2], providing energy to the atomic electrons of the sample which can then release as the secondary electrons (SEs), and backscattered electrons (BSEs) then the image can be formed by collecting these electrons from each point of the sample [29, 30]. The basic requirement for SEM to operate under a vacuum to avoid interactions of electrons with gas molecules in order to obtain high resolution [29].

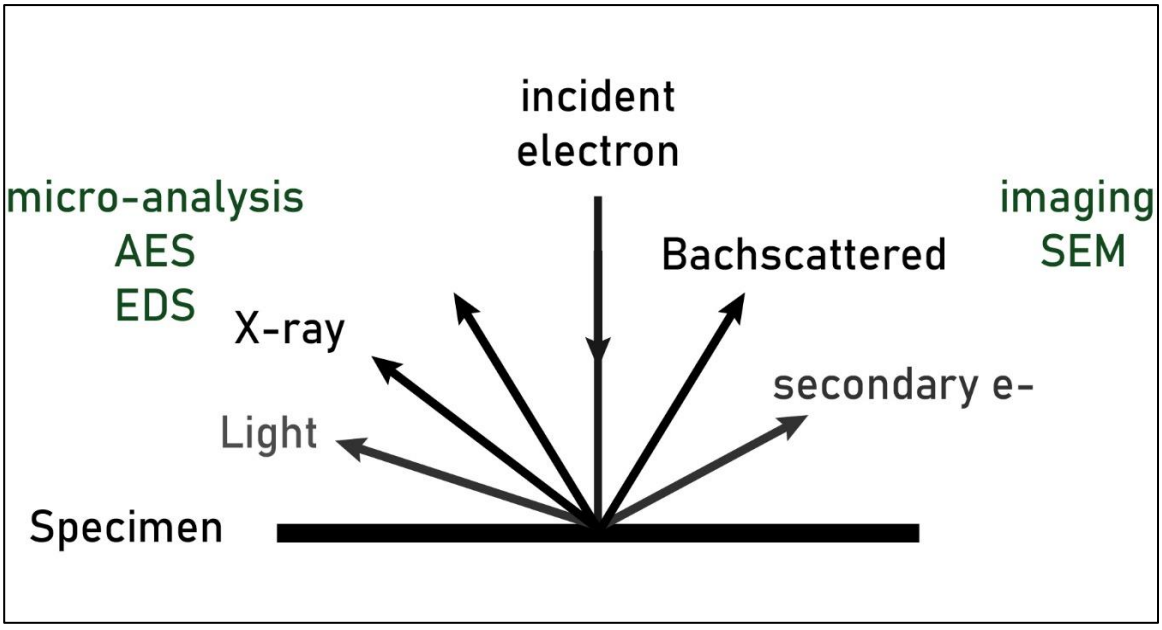

Figure II-8: Schematic representation of the interaction of a primary electron beam and the sample.

II.4.3.1.1 Energy dispersive X-ray spectroscopy (EDS or EDX):

The energy dispersive X-ray spectroscopy (EDS/EDX) is a technique for elemental analysis and chemical composition determination, associated with electron microscopy. The

method relies on the generation of characteristic X-rays, that reveals the identity of the elements present in the sample. Typically, this technique is used in conjunction with scanning electron microscopy [31].

As mentioned above, an incident electron beam hits atoms of the sample emitted secondary and backscattered electrons from the sample surface; however, these are not the only signals emitted from the sample. When the incident beam bounces through the sample creating secondary electrons, it leaves thousands of the sample atoms with holes in the electron shells where the secondary electrons used to be. If these "holes" are in inner shells, the atoms are not in a stable state. To stabilize the atoms, electrons from outer shells will drop into the inner shells, nevertheless, because the outer shells are at a higher energy state, to do this the atom must lose some energy. It does this in the form of X-rays. The X-rays emitted from the sample atoms are characteristic in energy and wavelength to, not only the element of the parent atom, but which shells lost electrons and which shells replaced them, this permits the elemental composition of the sample to be measured. Thus, EDX spectrum not only identifies the element corresponding to each of its peaks, but also the type of X-ray to which it corresponds as well [25].

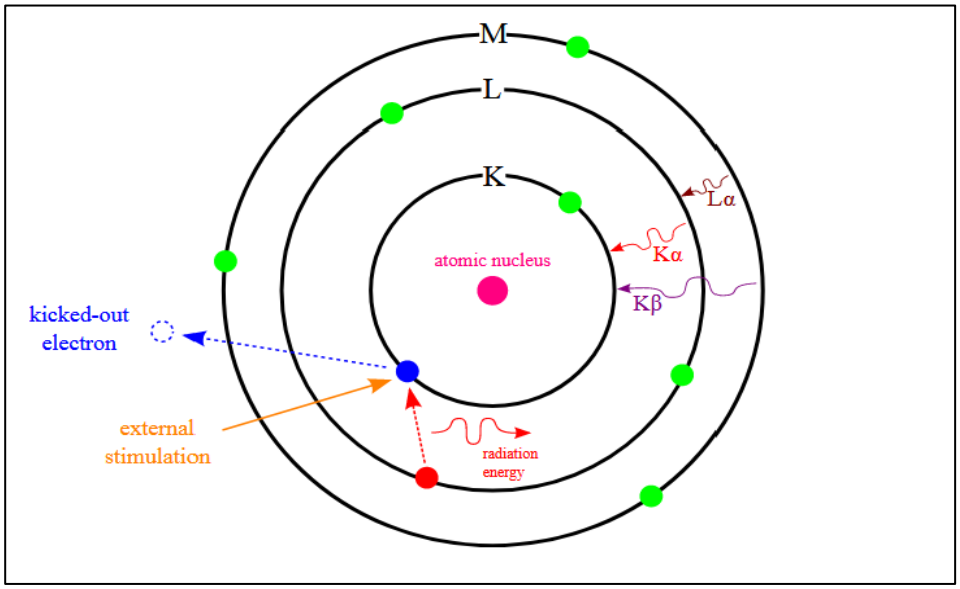

Figure II-9: Scheme of X-ray excitations in EDX analysis [25].

II.4.3.2 Stylus profilometry:

The stylus profilometry can provide us another characteristic which is measuring the surface roughness (RMS values) and providing a detailed 3D image of the sample surface. An example of 3D image is shown in figure II-10:

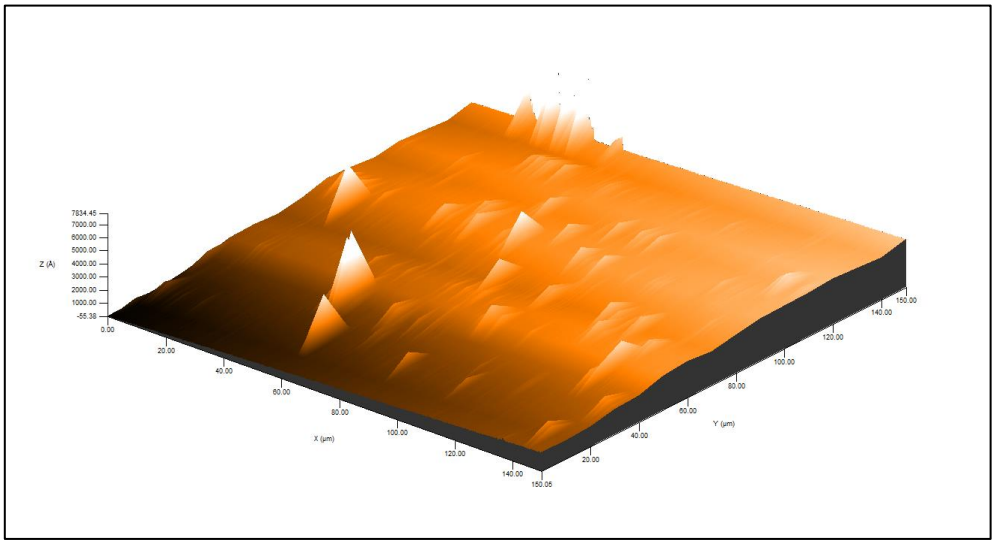

Figure II-10: 3D image of ZnO thin film elaborated by dip-coating and sol-gel method calcined at 500℃.

II.4.4 Optical characterization with spectroscopy (UV-Vis):

The optical characterization with ultraviolet-visible spectroscopy is a non destructive technique which measures the transmittance of an optical material in the UV-Vis and near-infrared spectral region, as well as other parameters like absorbance coefficient, the optical gap, refractive index, porosity, and Urbach energy.

The intensity of light passed through a sample, a part of it may be absorbed, while the rest will be transmitted through the thin film. Considering that, this sample is homogeneous with thickness (d), so it follows Beer-Lambert's law [2] (II-15):

$$I = I_0 e^{-\alpha d} \qquad \text{(II-15)}$$

Where αis the absorption coefficient, I_0 and I are the intensity of the incident and the transmitted beams, respectively.

The transmittance is given by [2] (II-16):

$$T(\%) = \left(\frac{I}{I_0}\right) \times 100 \qquad \text{(II-16)}$$

The absorption coefficient α can be calculated by [2] (II-17):

$$\alpha = \left(\frac{1}{d}\right) \times \ln\left(\frac{1}{T}\right) [cm^{-1}] \qquad \text{(II-17)}$$

II.4.4.1 Optical band Gap:

One of the important properties of semi-conductor is the band gap, it can be defined as the energy difference between the top of the valence band (BV) and the bottom of the conduction

band (BC) [32]. The optical band gap of a given thin film is determined by applying the Tauc model, and the Davis and Mott model in the high absorbance region (II-18) [26]:

$$(\alpha h\nu) = A(h\nu - Eg)^n \qquad \text{(II-18)}$$

where (hν) is the photon energy, Eg the optical band gap, and A is a constant. For n=1/2 the transition data provide the best linear curve in the band-edge region, implying the direct transition. The band gap of the films can be deduced from a plot $(\alpha h\nu)^2$ versus photon energy (hν) and extrapolating the straight line portion of this plot to the energy axis as presented in Figure II-11 [26]:

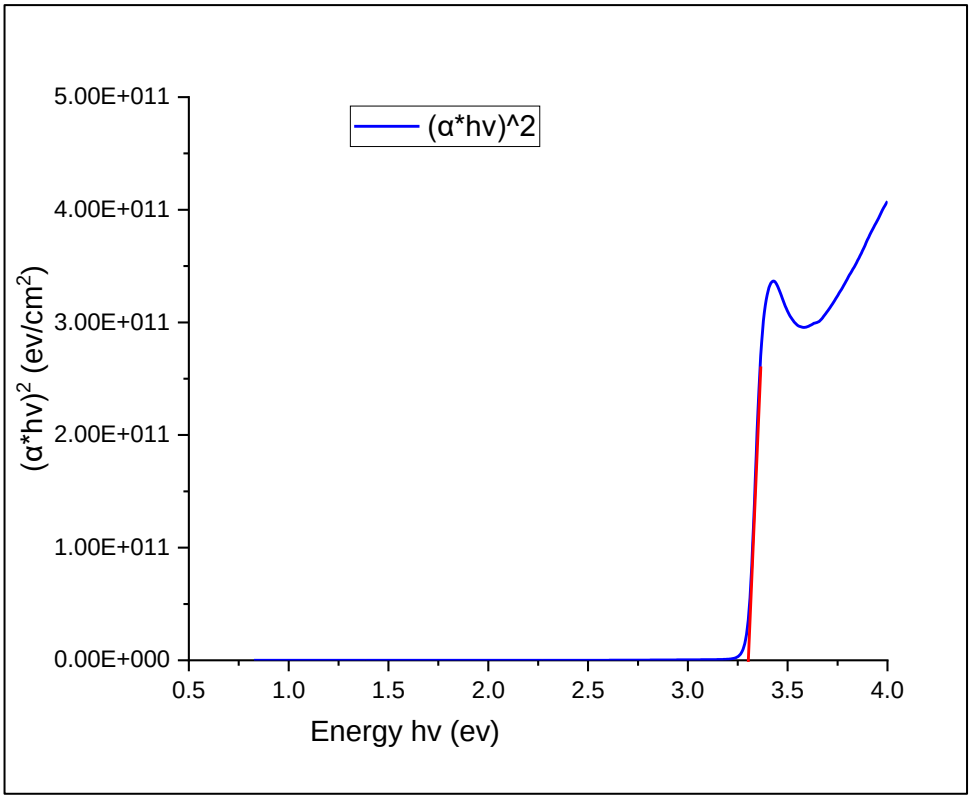

Figure II-11: Tauc model.

II.4.4.2 Urbach energy (Band tail):

The optical absorption spectra of semiconducting materials have an important role because it affords the basic information about its composition and optical band gap. The optical absorption spectra of the semiconductor can be divided into three main regions; they are (1) weak absorption region, which arise from defects and impurities, (2) absorption edge region, that arise due to perturbation of structural and disorder of the system, and (3) the region of strong absorption that determines the optical energy gap. Along the absorption coefficient curve and

near the optical band edge, there is an exponential part called Urbach tail [33-35], as show in Figure II-12. This tail can be formed during the transition process of electron. Generally, in optical absorption, near band edges, an electron from the top of the BV gets excited into the bottom of BC. During this transition process, if these electrons encounter disorder, it causes density of their states ρ(hν), where (hν) is the photon energy, tailing into the energy gap. This tail of ρ(hν) extending into the energy band gap is termed as Urbach tail [34].

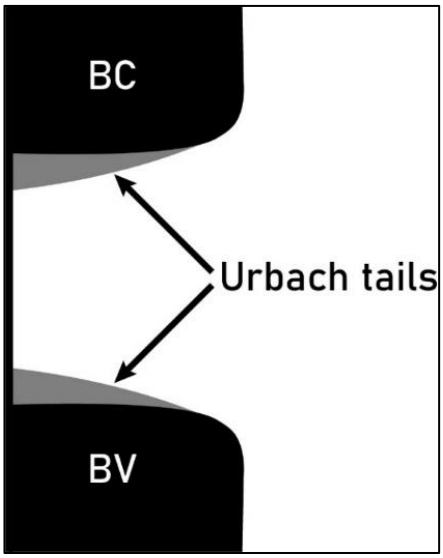

Figure II-12: Urbach tail scheme.

This exponential tail appears in the low crystalline, poor crystalline, the disordered, and amorphous materials because these materials have localized states which extended in the band gap. In the low photon energy range, the spectral dependence of the absorption coefficient (α) and photon energy (hν) is known as Urbach empirical rule, that is given by the following equation (II-19) [33]:

$$\alpha = \alpha_0 e^{\left(\frac{h\nu}{E_u}\right)} \qquad \text{(II-19)}$$

Where α_0 is a constant and $E_u$is Urbach energy or Urbach tail [33].

Taking the logarithm of the two sides of the last equation, hence one can get a straight line equation. It is given as follows (II-20) [33]:

$$\ln(\alpha) = \alpha_0 + \left(\frac{h\nu}{E_u}\right) \qquad \text{(II-20)}$$

Therefore, E_u can be estimated from the inverse slope of the linear plot between ln (α) versus (hν) (Figure II-13).

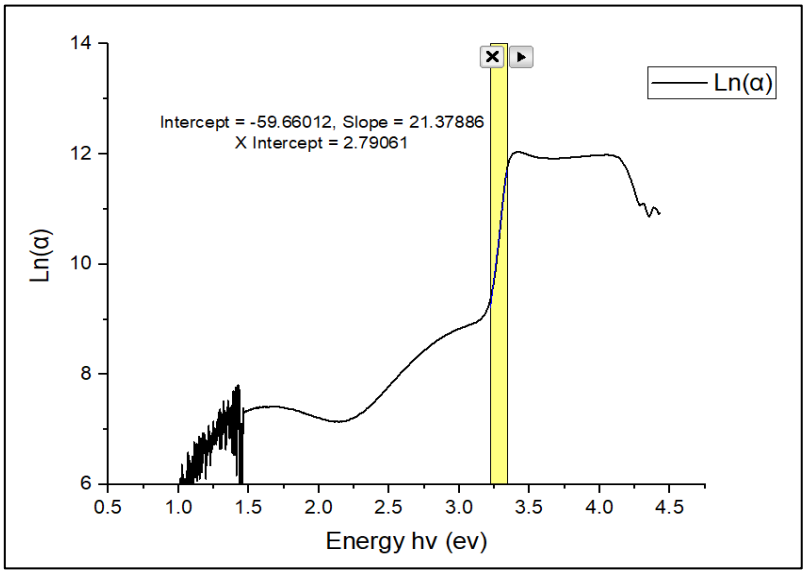

Figure II-13: Urbach energy.

II.4.4.3 Refractive index:

the optical and electronic behavior of semiconductors are decided by two fundamental properties namely energy gap and refractive index [38]. The refractive index of the film can be calculated from the following Herve and Vandamme relation (II-21) [36-38]:

$$n = \sqrt{1 + \left(\frac{A}{E_g + B}\right)^2} \qquad \text{(II-21)}$$

Where A and B are numerical constants with values of 13.6 and 3.4 eV respectively.

II.4.5 Electrical characterization techniques:

II.4.5.1 Four points probes method:

The most commonly used instrument for the measurement of resistivity of semiconductor samples is the four points probes. This technique uses 4 probes arranged along a straight line and equally spaced as indicated in Figure II-14. A current source forces a constant electrical current I [A] through the external needles, and the current is measured by an ammeter. A voltmeter at same time measures the voltage V [V] produced between the inner needles [39]. In thin film case with a thickness $t \ll d$, it's resistivity is given by (II-22):

$$\rho = \frac{\pi}{\ln(2)} \times t \times \frac{\Delta V}{I} = 4.532 \times t \times \frac{\Delta V}{I} \ [\Omega.\mathrm{cm}] \qquad \text{(II-22)}$$

The conductivity can be calculated from the following formula (II-23):

$$\sigma = \frac{1}{\rho} \ [\Omega.\,cm^{-1}] \qquad \text{(II-23)}$$

The main limitation of four points probe is that for thin film measurements the current has to be confined within the layer, usually requiring an insulating layer or junction underneath to prevent current leakage through the substrate [40].

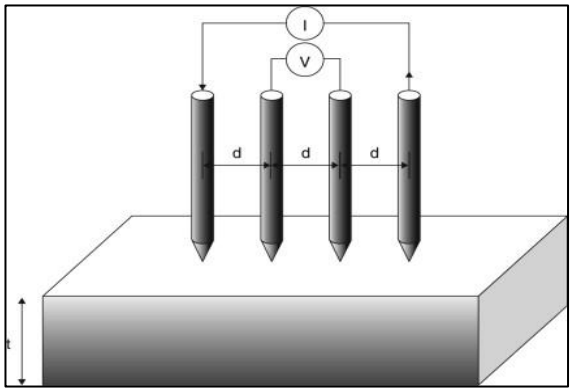

Figure II-14: Schematic representation of a four points probe [39].

II.4.5.2 Two points probe method:

The two points probes method can offer measuring resistivity of high resistivity samples. In this method, a current I [A] is injected and the resulting voltage drop V [V] is measured, the conductivity can be calculated by (II-24) [2]:

$$\sigma = \frac{1}{\rho} = \frac{L}{R.\,h.\,w} \ [\Omega.\,cm^{-1}] \qquad \text{(II-24)}$$

Knowing that:

- **ρ** is the resistivity of the film.
- **R** is the resistance of the film.
- **L** is the distance between the two probes.
- **W** is the thickness of the film.
- **h** is the width of the film.

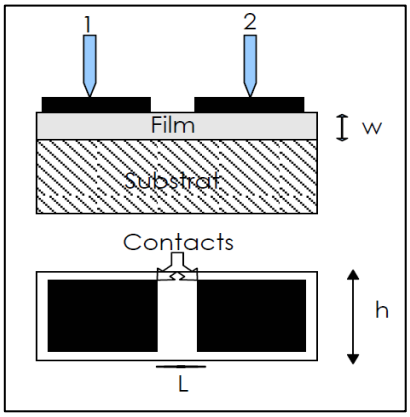

Figure II-15: Schematic representation of a two points probe [2].

II.4.5.3 Advantage of four probes method over two probes method:

Four points probe is preferred than two-point probe, as the contact and spreading resistances in two points probes are large and the true resistivity cannot be actually separated from measured resistivity [20]. In the four points probe method, contact and spreading resistances are extremely low with voltage probes and hence accuracy in measurement is usually very high. To measure very low resistance values, four probe method is used. Also, two points probes cannot be used for randomly shaped samples [20].

II.4.5.4 Figure of merit:

The coexistence of low electrical resistivity and excellent optical transparency ultimately leads to high figure of merit, which made it an important parameter to explore the applicability of any transparent conductor, which means studying the electro-optical performance of TCO [41,42]. The figure of merit is defined by [42]:

$$\varphi_{TC} = \frac{T^{10}}{R_{sh}} \qquad \text{(II-25)}$$

Where T is the total visible transmittance at λ= 550 nm and R_{sh} is the sheet resistance [42].

REFERENCES

[1] Adl Ahmad.H, Synthesis and Characterization of Solution Processed ZnO Thin Films, Doctoral Thesis, University of Alberta, Canada (2016).

[2] Saâd Rahmane, Elaboration et caractérisation de couches minces par spray pyrolyse et pulvérisation magnétron, Doctoral Thesis, Biskra University Algeria (2008).

[3] J. Livage, D. Ganguli, Sol-gel electrochromic coatings and devices: A review, Solar Energy Materials & Solar Cells 68 (2001) 365-381.

[4] H. Bahadur, A. K. Srivastava, R. K. Sharma, S. Chandra, Morphologies of Sol–Gel Derived Thin Films of ZnO Using Different Precursor Materials and their Nanostructures, Nanoscale Res. Lett. (2007) 2:469–475, DOI 10.1007/s11671-007-9089-x.

[5] MAACHE Mostefa, Elaboration de films minces d'oxydes semiconducteurs par voie Sol-Gel, Doctoral Thesis, Biskra University Algeria (2014).

[6] L. Yang, Fabrication and characterization of micro lasers by the Sol-Gel method, Doctoral Thesis, California institute of technology, Pasadena, California, USA, (2005).

[7] T. Schneller, R. Waser, M. Kosec, D. Payne, Deposition Techniques, Chemical Solution Deposition of Functional Oxide Thin Films, Springer-Verlag Wien, (2013).

[8] L. Znaidi, Sol–gel-deposited ZnO thin films: A review, Materials Science and Engineering B 174 (2010) 18–30.

[9] I. Limón-Rocha, C. A. Guzmán-González, Luis M. Anaya-Esparza, R. Romero-Toledo, J. L. Rico, O. A. González-Vargas, A. Pérez-Larios, Effect of the Precursor on the Synthesis of ZnO and Its Photocatalytic Activity, Inorganics 2022, 10, 16

[10] M. Ohyama, H. Kozuka, T. Yoko, S. Sakka, Preparation of ZnO Films with Preferential Orientation by Sol-Gel Method, J. Ceram. Soc. Jpn. 104 (1996) 296–300.

[11] S. Chakrabarti, D. Ganguli, S. Chaudhuri, Substrate dependence of preferred orientation in sol–gel-derived zinc oxide films, Materials Letters 58 (2004) 3952– 3957.

[12] X. Tang, X. Yan, Dip-coating for fibrous materials: mechanism, methods and applications, J Sol-Gel Sci. Technol., (2017), DOI 10.1007/s10971-016-4197-7

[13] CJ. Brinker, AJ. Hurd, GC. Frye, PR. Schunk, CS. Ashley, Sol-gel thin film formation, J Ceram Soc Jpn, (1990), 862–877.

[14] M. Faustini, B. Louis, PA. Albouy, M. Kuemmel, David. Grosso, Preparation of Sol-Gel Films by Dip-Coating in Extreme Conditions, J. Phys. Chem. C, Vol. 114, No. 17, (2010).

[15] I.M Thomas, Optical Coating Fabrication: Sol-Gel Optics, The Springer International Series in Engineering and Computer Science, vol 259, (1994), 140-156.

[16] A. Piergari, E. Masetti, Thin film thickness measurement: a comparison of various techniques, Thin Solid films, 124, (1985) 249-257.

[17] N. Kouidri, S. Rahmane, Effect of cobalt chloride concentration on structural, optical and electrical properties of Co_3O_4 thin films deposited by pneumatic spray, J. New Technol. Mater, Vol. 10, N°01 (2020) 56-62.

[18] A. Allag, S. Rahmane, A. Ouahab, H. Attouche, N. Kouidri, Optoelectronic properties of SnO2 thin films sprayed at different deposition times, Chin. Phys. B Vol. 25, No. 4 (2016) 046801.

[19] R. Swanepoel, Determination of the thickness and optical constants of amorphous silicon, J.Phys. E Sci. Instrum, (1983), 16, 1214–1222.

[20] زوبيري بلال، دراسة خصائص الشرائح الرقيقة لأكسيد الزنك المحضرة بطريقة الرش بالهواء المضغوط انطلاقا من مصادر مختلفة للزنك، مذكرة ماستر، جامعة بسكرة، (2021).

[21] R. Kohli, K.L. Mittal, Methods for Assessing Surface Cleanliness, Developments in Surface Contamination and Cleaning, Volume 12, Elsevier Science (2019), 23-105.

[22] N. Fleck, H. Amli, V. Dhanak, A. Waqar, Characterization techniques in energy generation and storage, Emerging Nanotechnologies for Renewable Energy, Elsevier, (2021), 259-285.

[23] He. Kaliyan Rao, T.N. Srinivasa, R.S. Kulkarni, A.R, High performance varistors prepared from doped ZnO nanopowders made by pilot-scale flame spray pyrolyzer: Sintering, microstructure and properties. Journal of the European Ceramic Society, 35 (2015) 3535–3544.

[24] P. Scherrer, Bestimmung der Größe und der inneren Struktur von Kolloidteilchenmittels Röntgenstrahlen, Nachr. Ges. Wiss. Göttingen 26 (1918), 98-100.

[25] Yahia Anouar, Optimization of indium oxide thin films properties prepared by sol gel spin coating process for optoelectronic applications, Doctoral Thesis, Biskra University Algeria (2019-2020).

[26] S. Rahmane, A. Mohamed Salah, M. Abdou Djouadi, N. Barreau, Effects of thickness variation on properties of ZnO:Al thin films grown by RF magnetron sputtering deposition, Superlattices and Microstructures, 79, (2015),148–155.

[27] F. Siti, R. Ragadhita, D. Fitria Al Husaeni, A. Bayu Dani Nandiyanto, How to Calculate Crystallite Size from X-Ray Diffraction (XRD) using Scherrer Method, ASEAN Journal of Science and Engineering 2 (1) (2022) 65-76.

[28] Z. Raza Khan, M. Shoeb Khan, M. Zulfequar, M. Shahid Khan, Optical and Structural Properties of ZnO Thin Films Fabricated by sol-gel Method, Material Sciences & Applications, (2011), 2, 340-345

[29] Akhtar K, Khan S.A., Khan S.B., Asiri A.M, Scanning Electron Microscopy: Principle and Applications in Nanomaterials Characterization, Handbook of Materials Characterization, Springer (2018).

[30] H. Garbacz, A. Królikowski, Corrosion resistance of nanocrystalline titanium, Nanocrystalline Titanium, Elsevier, (2019).

[31] K. Torres-Rivero, J. Bastos-Arrieta, N. Fiol, A. Florido, Metal and metal oxide nanoparticles: An integrated perspective of the green synthesis methods by natural products and

waste valorization: applications and challenges, Comprehensive Analytical Chemistry, Elsevier, Volume 94, (2021), 433-469,

[32] O.A. Jianu, G.F. Naterer, M.A. Rosen, Igor L. Pioro, 19, Hydrogen cogeneration with Generation IV nuclear power plants, Hand book of Generation IV Nuclear Reactors, Woodhead Publishing, (2016), 637-659.

[33] A.S. Hassanien, A. Alaa Akl, Effect of Se addition on optical and electrical properties of chalcogenide CdSSe thin films, Superlattices and Microstructures, 89, (2016) 153-169.

[34] N. Sharma, S. Sharma, K. Prabakar, S. Amirthapandian, S. Ilango, S. Dash, A. K. Tyagi, Optical band gap and associated band-tails in nanocrystalline AlN thin films grown by reactive IBSD at different substrate temperatures, Material Science Group, Indira Gandhi Centre for Atomic Research,1507.04867 (2015).

[35] F. Urbach, the Long-Wavelength Edge of Photographic Sensitivity and of the Electronic Absorption of Solids, Physical Review, 92(5), (1953), 1324–1324. doi:10.1103/physrev.92.1324.

[36] S.K. Tripathy, Refractive indices of semiconductors from energy gaps, Optical Materials, 46 (2015), 240–246.

[37] A. Allag, S. Rahmane, N. Kouidri, H. Attouche, A. Ouahab, Polycrystalline SnO_2 thin films grown at different substrate temperature by pneumatic spray, J Mater Sci: Mater Electron, (2017) 28:4772–4779.

[38] P. Hervé, L. K. J. Vandamme, General relation between refractive index and energy gap in semiconductors, Infrared Phys. Technol. 35, 609, (1994).

[39] R. Miranda, Characterization of FSP by electrical conductivity: Surface Modification by Solid State Processing, Woodhead Publishing, (2014), 153-176.

[40] T. Markku, M. Teruaki, A. Veli-Matti, S. Franssila, M. Paulasto-Kröckel, L. Veikko, Silicon Wafer and Thin Film Measurements: Hand book of Silicon Based MEMS Materials and Technologies (Second Edition), William Andrew Publishing, (2015), 381-390.

[41] B. Sarma, D. Barman, K. Bimal Sarma, AZO (Al:ZnO) thin films with high figure of merit as stable indium free transparent conducting oxide, Applied Surface Science, 479, (2019) 786–795.

[42] G. Haacke, New figure of merit for transparent conductors, Journal of Applied Physics, 47, 4086 (1976); doi: 10.1063/1.323240

Chapter III:

Experimental part and discussion.

III.1 Introduction:

This chapter contains the elaboration of zinc oxide thin films, we present the choice of zinc oxide, includes a description of the choice and preparation of substrates and solution.

In addition to all experiment details and the conditions of preparations and analysis the deposited films using the characterization tools, we were also interested in the study of the transformation of their properties with the variation of the calcination temperature.

III.2 Elaboration of ZnO thin films:

III.2.1 The choice of zinc oxide:

Most of the recent interests on ZnO material have been focused on the future potentials of UV-blue light emitting devices (LED) and UV-blue lasers. The most desirable features of ZnO can be listed as follows:

1. ZnO has the extremely large exciton binding energy of $(60\ \text{meV})$ which is much greater than the thermal energy $(26\ \text{meV})$ at room temperature. This energy considered as an important parameter that enables the UV laser diode, and other exciton related light emitting devices to be two operated at room temperature.
2. High transparency in the visible and near infrared spectral region.
3. ZnO is one of the "hardest" materials in II-VI compound semiconductors due to the higher melting point and larger cohesive energy. It can be expected that a degradation of the material due to the generation of dislocations during the device operation will be reduced.
4. Low material costs, nontoxicity, and abundance in the earth crust.
5. Interfacial energy between ZnO and sapphire or other oxide substrates is such that two-dimensional growth is favored, which results in high quality films at lower temperature.
6. Possibility to prepare highly doped films with free electron density $(\text{n} > 10^{20}\text{cm}^{-1})$ and low resistivity $(< 10^{-3}\ \Omega\,.\,\text{cm})$.
7. Good contact to the active semi-conductors (absorber layers).
8. Possibility to prepare the TCO layer on large areas $(> 1\ \text{m}^2)$ by deposition methods.
9. Possibility to prepare ZnO films with suitable properties at low substrate temperature [1].

III.2.2 The choice of substrate:

The choice of substrate is very important to the properties of the thin film, since it affects crystalline quality as well as optical and electrical properties of ZnO film [2]. In this work, the thin films of ZnO were deposited on glass slides in a size of $(25.4 \times 76.2)\ \text{mm}$ and $(1\ \text{to}\ 1.2\ )\ \text{mm}$ thickness this choice was due to these reasons:

- This glass performs a good optical characterization of our films, due to its transparency in UV-Visible wavelength range.
- It must be an isolator layer so it will not affect the conductivity measurement.
- To minimize the thermal stresses because the two materials constituting the sample (glass + zinc oxide) have a very close thermal dilatations coefficients [1,2].
- For economic reasons.

III.2.3 Cleaning and preparation of substrate:

The properties of such a deposited film depend on the cleanliness of the substrate surface on which the film is deposited. Contamination on this surface can result in reduced adhesion of the film to the substrate [3], thus it is necessary to remove contamination, which include finger prints, dust, oil, and lint particles, and verify that the surface of substrate does not have any damage.

The steps of cleaning the surface of substrate is:

- Washing it with distilled water and soap.
- Drying using absorbent paper.
- Acetone bath during 10 min to eliminate the organic impurities. Then washing it with distilled water [4].
- Ethanol bath during 10 min. Then washing it with distilled water.
- Drying using absorbent paper.
- Drying using a drier.
- Drying using absorbent paper.

III.2.4 The solution's preparation:

ZnO thin films were prepared by the sol-gel dip-coating method on the glass substrates. The solution (A) made by dissolving Zinc acetate ($Zn[OOCCH_3]_2.2H_2O$) as a starting material (precursor) in Ethylene glycol (EG) as a solvent. This solution heating at 120 °C for 20 minutes until the obtainment of the transparent gel, and the concentration of zinc acetate was 0.6 M. At the same time, preparing another solution (B) by adding Propanol-1 and water (H_2O) as solvents, and Monoethanolamine (MEA) as a stabilizer. Moreover, the solution was stirred at room temperature for 15 minutes. After that, we waited the solution (A) until the gel cools down, then we added Propanol-1, and hold on while the gel is completely dissolved. Where a mixture of small drops of glycerol, that act as a soluble, and solution (B) were amplified to the gel. The resulting mixture was stirred at room temperature for 2 days (48 hours) in order to yield definitely a clear and homogeneous sol-gel solution, which served as the coating solution.

III.3 The influence of calcination temperature on ZnO thin films:

III.3.1 Experimental details:

III.3.1.1 Dip coating device:

Holmarc's Dip Coating Unit with Infrared Dryer (HO-TH-02B) has been designed to keep operator involvement as minimum as possible so that variables like speed, duration, etc. are maintained accurately by micro processor controller.

The outstanding feature of this model is the presence of an Infrared dryer in it. Inside the unit, there is an infrared heater, which offers a maximum temperature of 200°C from ambient. After each dip, the Infrared heater helps in drying the substrate. It provides uniform heating to the substrate. The temperature is swiftly attained so that the time taken for the dipping process is greatly reduced. The coating thickness can be easily controlled by adjusting the withdrawal rate and the viscosity of the coating solution.

Another advantage of this model is that it minimizes the energy consumption as the heater will be activated only after detecting the substrate, and hence it can provide the substrate with accurate temperature [5].

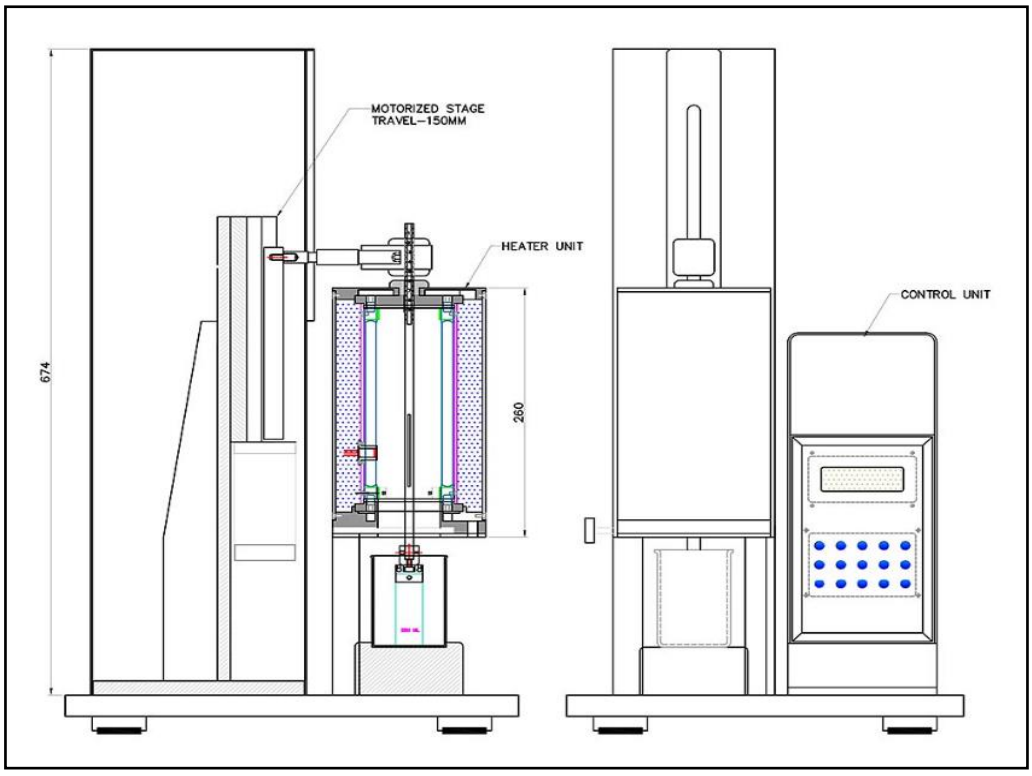

Figure III-1: Design of dip coating model No: HO-TH-02B [5].

III.3.1.2 Thin films deposition:

Dip coating technique is a process in which the substrate to be coated is immersed in a liquid, and then it is drawn at a well-defined drawing speed under a controlled temperature and device settings [6].

This part of the research involved the influence of calcination temperature on zinc oxide thin films. The conditions of dip coating deposition are described below in the Table III-1

Table III- 1: Table presents Holmarc's dip coating specifications.

Parameters	Values
Dry position	**10 mm**
Dip length	**140 mm**
Dip speed	**9 mm/s**
Retrieval speed	**9 mm/s**
Dip duration	**1 hour**
Dry duration	**10 minutes**
Numbers of dips	**2**
Dryer	**On**
Temperature	**200 °C**

After using dip coating process, the films were calcined at air in furnace at various calcination temperatures from 300 °C to 550 °C with a step of 50 °C for 2 hours, to induce densification and phase transformation.

There are a lot of parameters need to be considered in order to prepare high quality ZnO thin film for devices application and one of them is the calcination process. The calcination process not only leads to the reaction between film and substrate, but also improved the crystal structure of the film [7]. This research presents a study of the influence of calcination temperature on properties of ZnO thin films deposited on glass substrate using sol-gel dip-coating method.

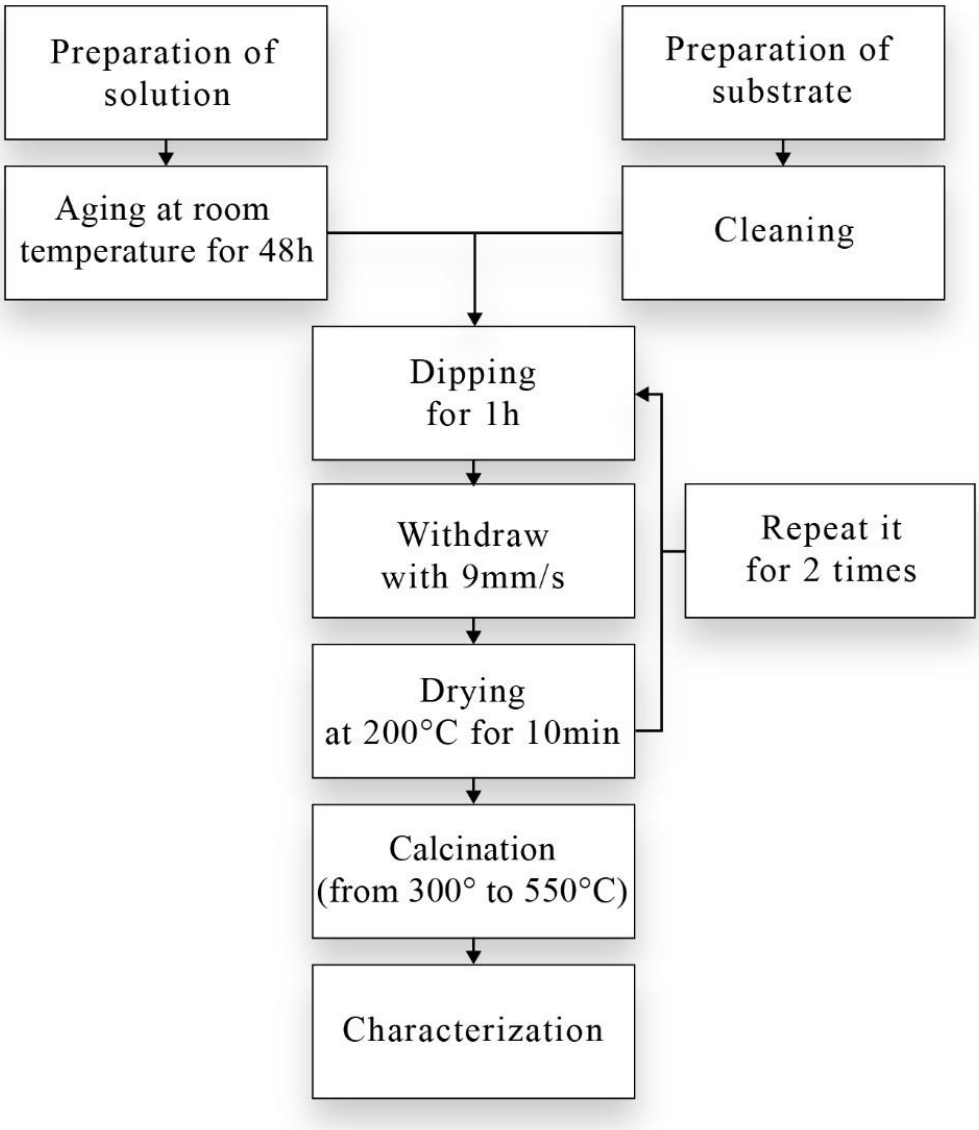

Figure III-2: A schematic representation of steps of thin film preparation and characterization in sol-gel process and dip-coating technique.

III.3.2 Results and discussion:

III.3.2.1 Film thickness calculation:

The film thickness of ZnO thin films, has been measured by the gravimetric method (mentioned in Chapter II) using a balance with the precision of 0.1 mg. Figure III-3 shows the plot of film thickness versus the calcination temperature, and it is clearly noticed that the thickness changes randomly with temperature.

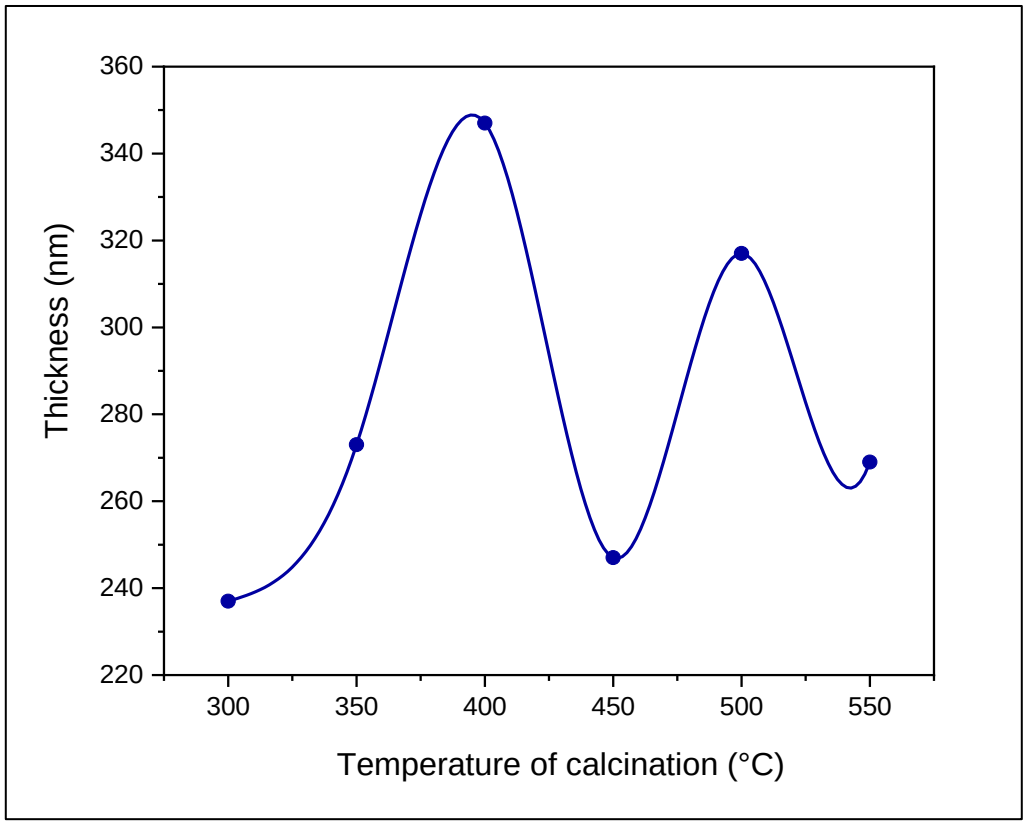

Figure III-3: Thickness variation of calcined ZnO thin films.

The thickness of the films was found to be between 240 and 350 nm, which considered as an inconsiderable change, this might be caused by the measurement error method and the conditions of the experiment, thus we can say that the thickness average is about 300 nm.

Where it can be explained, the decrease could be originated by the increment of material density owing to the evaporation of organic residual coming from the precursor solution [8]. It is difficult to control the growth of thin film during the process using the dip coating technique. The atmospheric conditions where the film growth takes place cannot controlled accurately.

III.3.2.2 Adhesion test:

The term adhesion refers to the interaction between the closely contiguous surfaces of adjacent bodies, i.e., a film and substrate. According to the American Society for Testing and Materials (ASTM), adhesion is defined as the condition in which valence forces hold two surfaces together, by mechanical anchoring, or by both together. Adhesion to the substrate is certainly the first attribute a film must possess before any of its other properties can be manifested or exploited. Even though its critical importance, adhesion is one of the least understood properties. The lack of a broadly applicable method for quantitatively measuring adhesion makes it virtually impossible to test any of the proposed theories for it.

The simplest and quickest qualitative measure of film or coating adhesion is Tape Test, which consists of:

An adhesive tape is applied to the film surface and pulled off again. The tape test is a subjective test, which is not only dependent on the type of tape but also on the pull off velocity and the pull off angle [9].

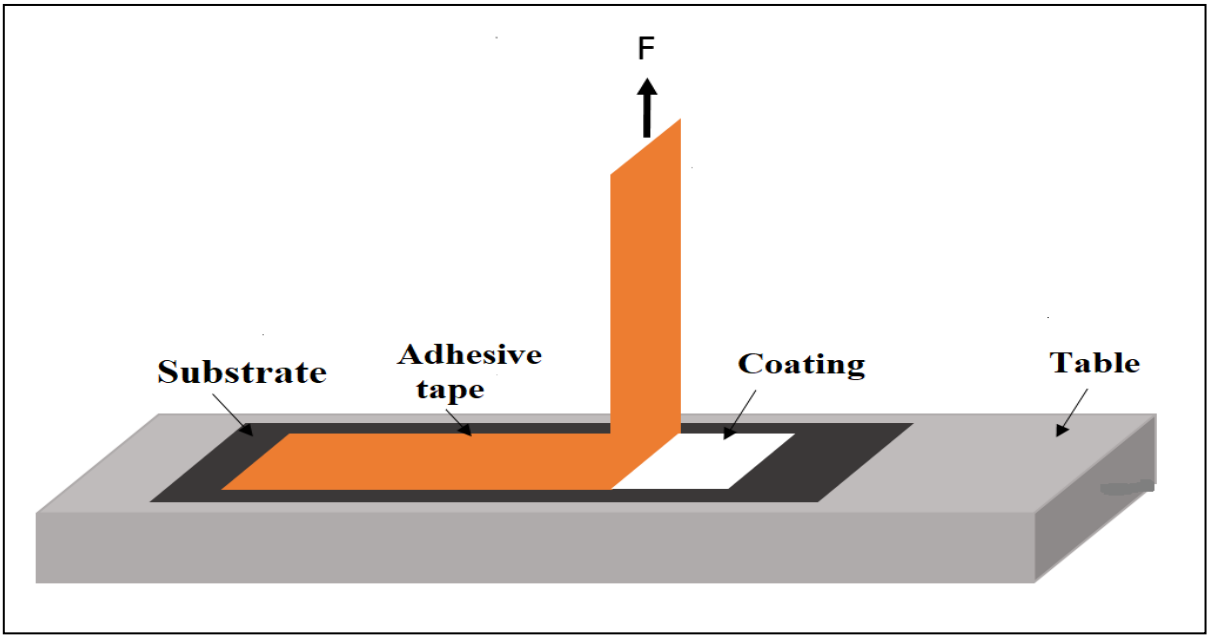

Figure III-4: Adhesive tape test [10].

For our films, we make the test above, while doing the adhesive tape test, we noticed that the coating is not removed, so we can say that the adhesion of the films is acceptable.

III.3.2.3 Structural characterization with XRD:

III.3.2.3.1 XRD analyses:

The structural analysis of the prepared ZnO thin films has been carried out using their X-ray diffraction (XRD) spectra (Rigaku MiniFlex 600). The XRD spectra have been obtained using CuKα radiation of wavelength 1.5406 Å in the 2θ. The X-ray diffraction study shows that the studied films are well crystallized in the preferred orientation (002), which indicates the hexagonal wurtzite crystal structure (JCPDS card No.036-1451) inserted in chapter II (Figure II-6). This preferential orientation is due to the low energy required for (002) plane formation [12].

The XRD patterns of the ZnO thin films calcined at different temperatures from 300°C to 550°C are displayed in Figure III-5. The presence of several major peaks (100), (002), (101) in the XRD spectra (Figure III-6) shows that all the films are polycrystalline in nature. Moreover, at the

highest temperature we can observe other peaks appears in addition of the three main peaks of zinc oxide, which are: (102), (110), (103), and (200) correspond to 2θ: 47.7°, 56.6°, 63°and 68° respectively (Figure III-5).

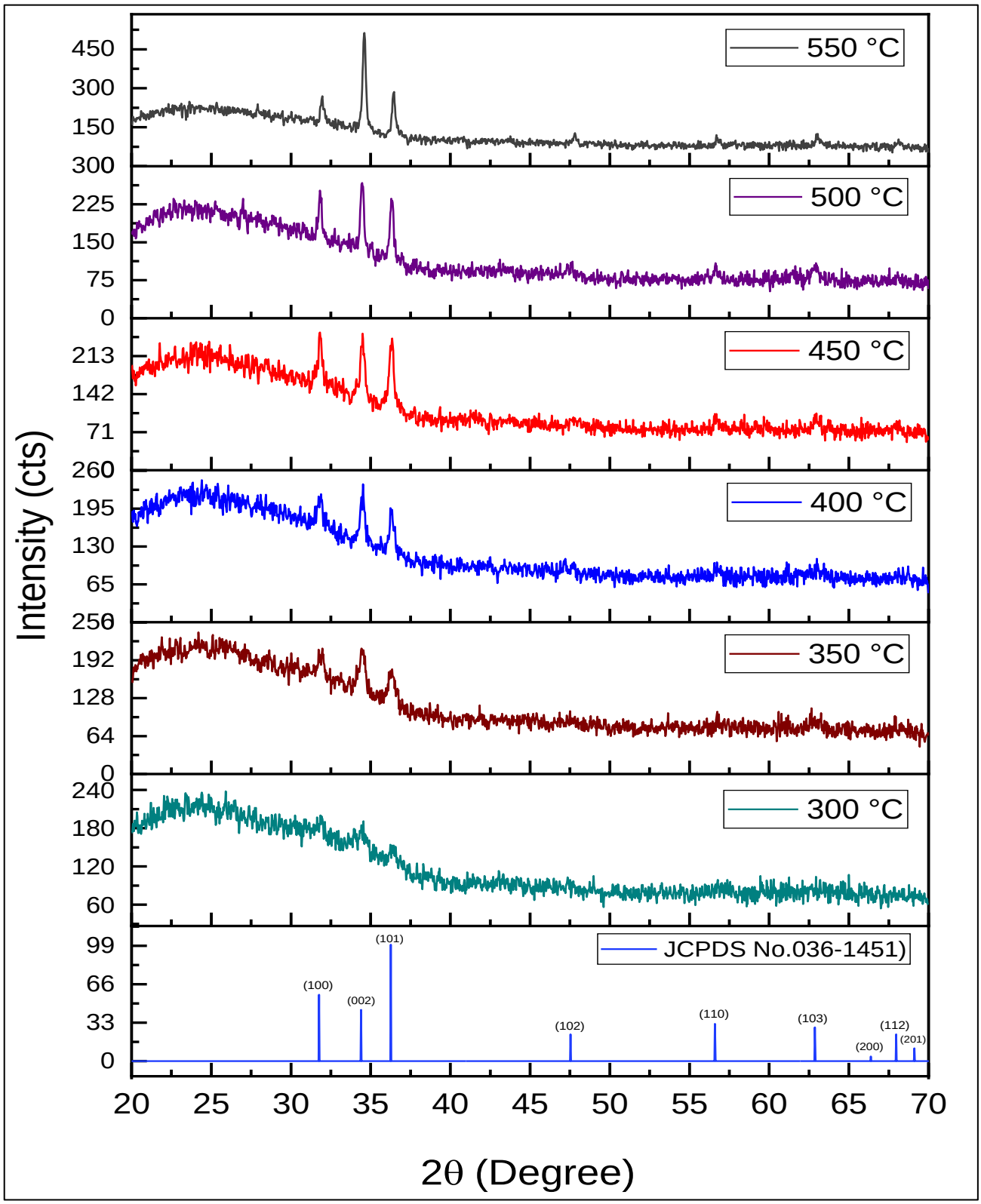

Figure III-5: X-ray diffraction spectra of ZnO thin films deposited at various calcination temperatures.

The orientation of ZnO thin films is dependent on calcination temperature, the sample calcined at 300°C showed poor crystallinity with a minor peak corresponding to minimum intensity at $2\theta = 34.40°$. However, when the calcination temperature increases, the (002) peak intensity is increasing; this means that calcination temperature can improve the crystallization quality of ZnO thin films. We can notice that there is a slight improvement in the intensity of the preferential peak of the films calcined at temperature 450 and 500°C, almost the same intensity in their peaks, this means that the recrystallization of materials begins at higher temperature, moreover, a large number of atoms move towards the (002) plane [11]. Those results agree well with [13,16].

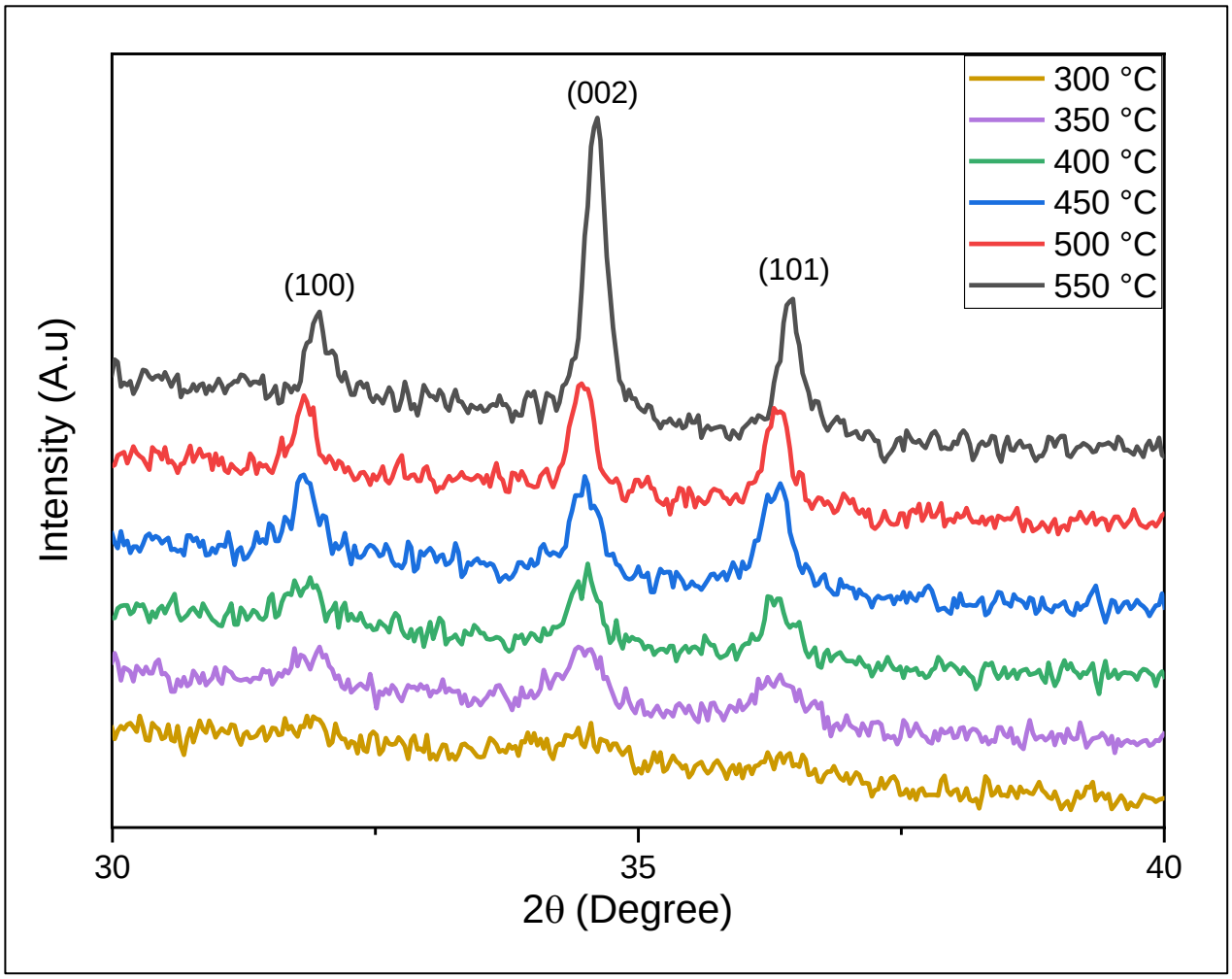

Figure III-6: Main XRD spectra at different temperature of calcination.

III.3.2.3.2 Crystallite size and Strain:

The strain and crystallite size of ZnO thin films were calculated from the peak (002), using the full width at half maximum (FWHM) in conjunction with the Debye–Scherer formula ((II-13), (II-14) in Chapter II). Figure III-7 shows the variation of strain and the crystallite size of the ZnO thin films with calcination temperatures, its values are inserted in Table III-2.

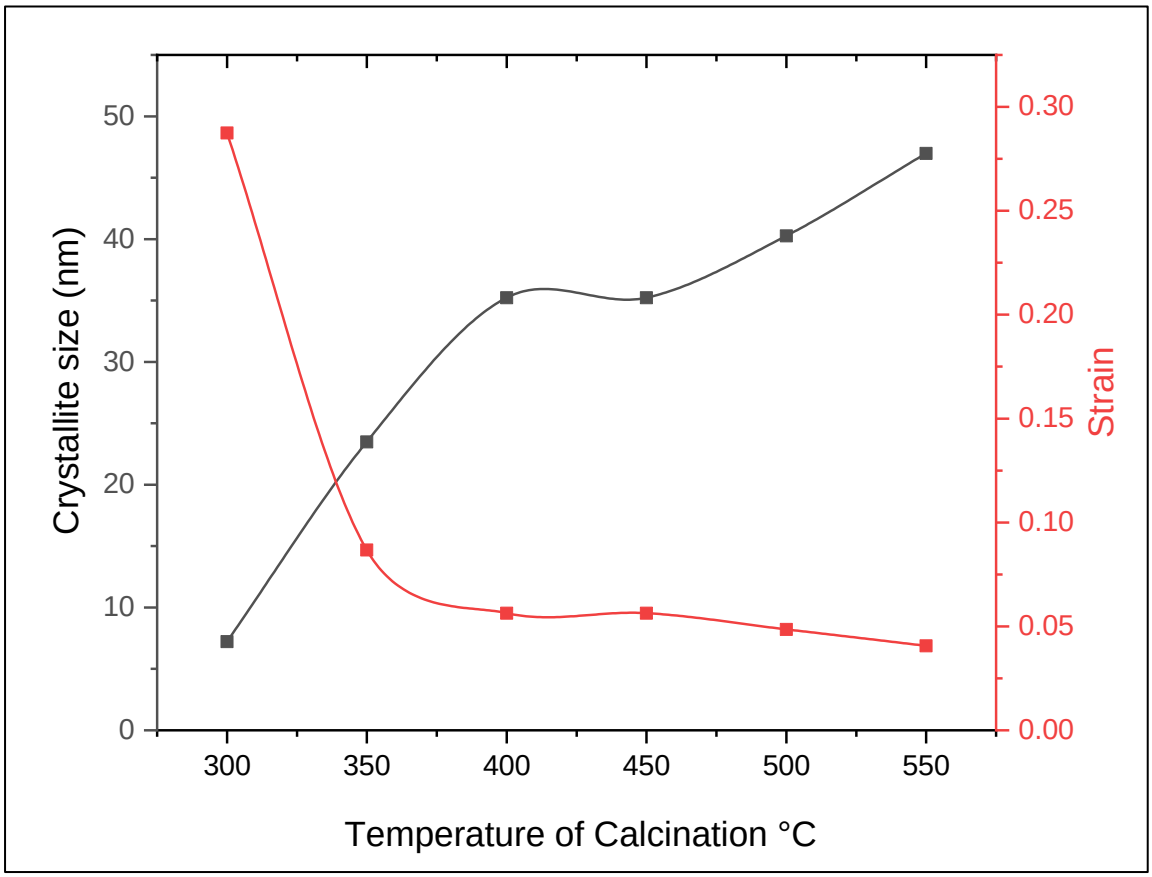

Figure III-7: Crystallite size and the strain as function of calcination temperatures.

It is easy to note that the crystallite size and the strain have an opposite variation. The observed augment in the crystallite size is commonly due to the decrease in the internal strain [8], the increase of the crystallite size of (002) plan has been indicated by the enhancement of the crystallinity [1].

In other way, from Table III-2 we observe that the FWHM decreases when the calcination temperature increases. Decreasing in the FWHM value leads to increase in crystallite size. [15] Also, found similar change in results. This may probably be attributed to the following: when the film atoms obtain enough energy in the calcination process, they will migrate and restructure into thin films. The crystallites then grow larger correspondingly [9].

Table III-2: Structural parameters values of ZnO thin films calcined at various temperatures.

Temperatures [°C]	2θ (002) [°]	2θ (100) [°]	FWHM	Crystallite size [nm]	Strain	d_{hkl} [Å]	C [Å]	a [Å]
300	**34.402**	**/**	**1.152**	**7.218**	**0.275**	**2.604**	**5.209**	**/**
350	**34.485**	**31.485**	**0.354**	**23.484**	**0.084**	**2.598**	**5.197**	**3.278**
400	**34.506**	**31.803**	**0.236**	**35.218**	**0.056**	**2.597**	**5.194**	**3.246**
450	**34.482**	**31.832**	**0.236**	**35.216**	**0.056**	**2.598**	**5.197**	**3.243**
500	**34.523**	**31.836**	**0.206**	**40.266**	**0.049**	**2.595**	**5.191**	**3.243**
550	**34.605**	**31.942**	**0.177**	**46.983**	**0.042**	**2.589**	**5.179**	**3.232**

The lattice constant C and a of ZnO thin films calculated (see Table III-2) seems that it is close to the lattice constant of bulk ZnO ($C_0 = 5.206$ Å, $a_0 = 3.249$ Å) indicating the strain is along the c-axis from defects and lattice distortions in the crystal.

Also, we noted that the d_{hkl} values are different from the reference ($d_{hkl} = 2{,}603$ Å); this variation in the values of d_{hkl} gives rise to the shift of the position of the peaks, which is probably caused by the manifestation of the strain during the growth of our film [14]. At high temperature, atoms have more energy to acquire a correct site in the crystal lattice [1]; this observation shows that the films have a high crystallinity with low strain.

III.3.2.4 Morphology:

Figure III-8 shows the surface morphology of ZnO thin films with different calcination temperatures characterized by Profilometry (KLA Tencor p-7). The 3D image clearly shows that the films are uniform. The scans of the few areas on the films surface shows the root mean square (RMS) roughness were 1.40, 8.33 and 15.8 nm for 300°C, 450°C and 500°C respectively. The sample with a calcination of 300°C shows a smooth and low surface roughness, these results revealed that the RMS roughness value of calcined ZnO films increased with the increasing of calcinations temperature. The result is almost similar to the study conducted by [7,4].

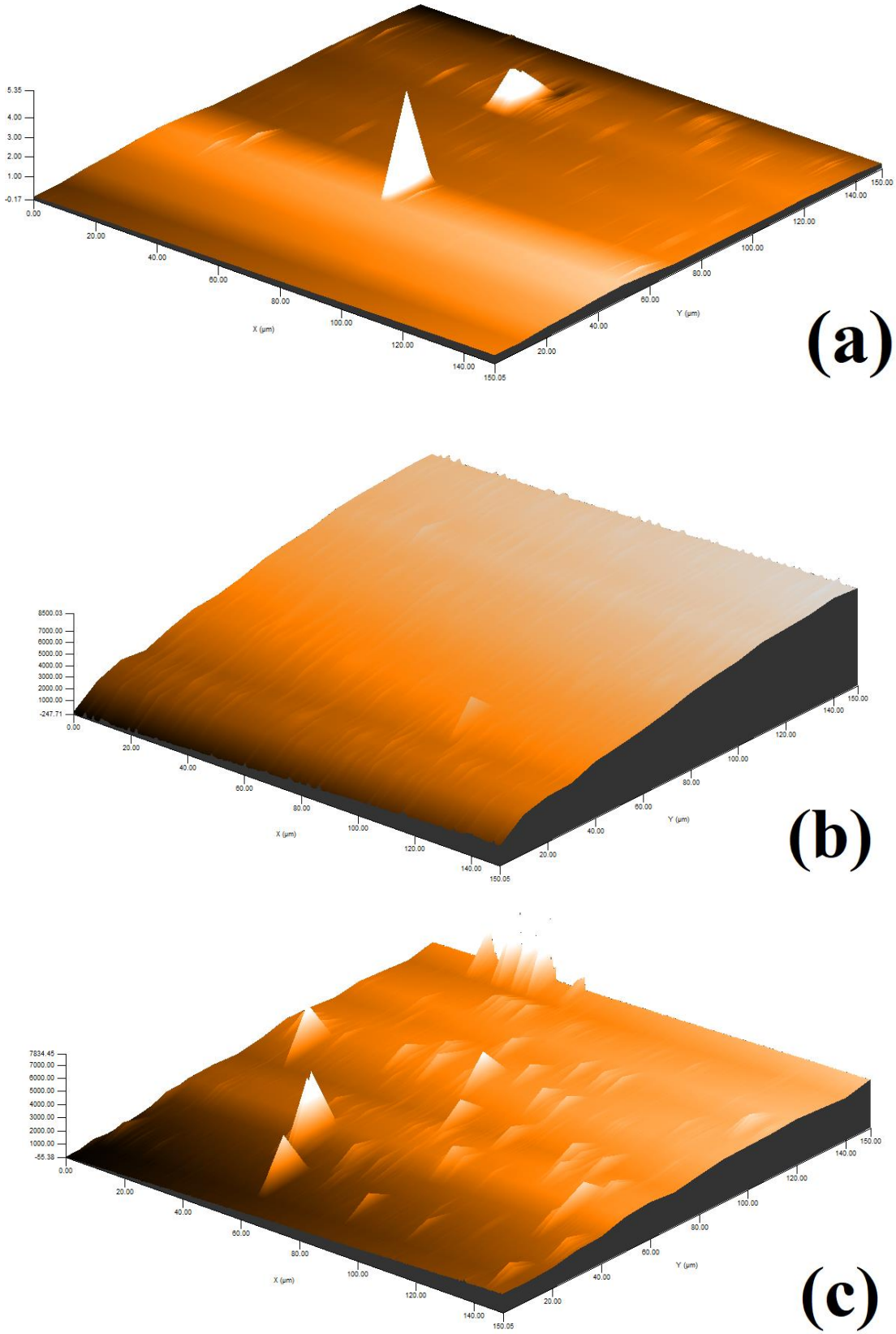

Figure III-8: Profilometry images of ZnO thin films deposited at different calcination temperatures: (a): T = 300°C; (b): T = 450°C; (c): T = 500°C

III.3.2.5 Optical characterization:

Optical properties of ZnO thin films are investigated by using JASCO V-770 spectrophotometer in the wavelength range [280-1500 nm] at room temperature.

III.3.2.5.1 Transmittance:

Figure III-9 displays the optical transmittance specters of ZnO thin films calcined at various temperatures (300-550°C). This spectrum shows two important zones which are the fundamental absorption and the interference oscillation region, the data point near the absorption edge can be used to determine the band gap of the semiconductor film using Tauc's model [18]. Second region can be used to determine the thickness of our thin films using the interference fringes as mentioned in the second chapter.

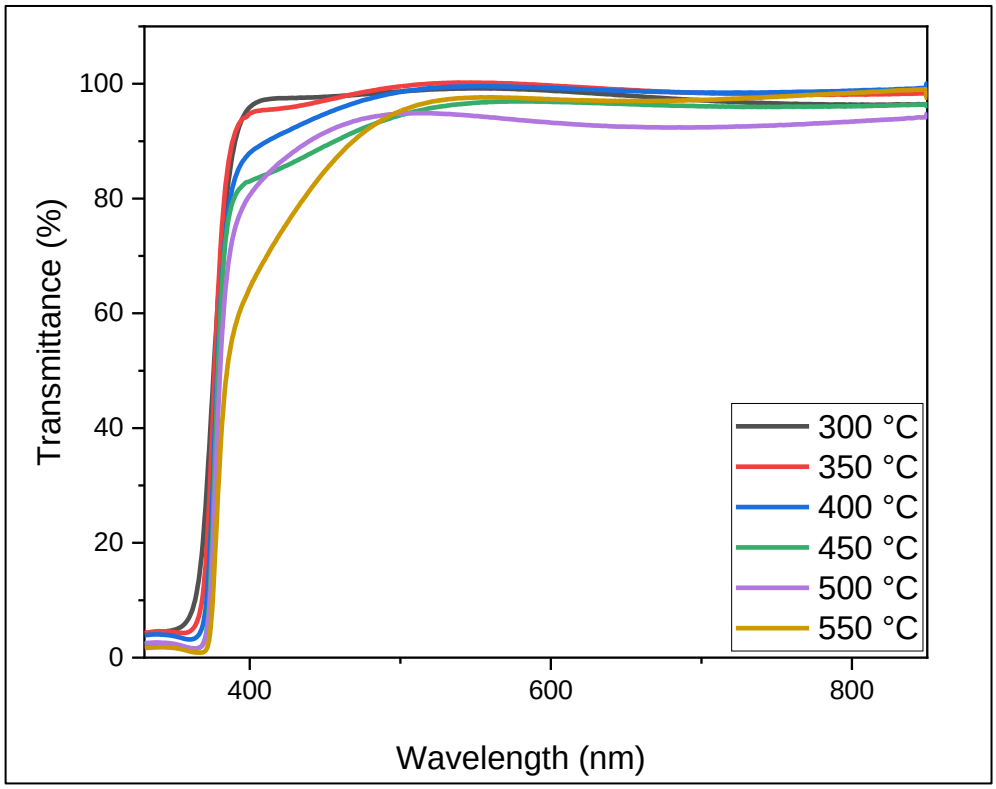

Figure III-9: Transmittance of ZnO thin films calcined at various temperatures.

From the specters above, it is observed that these thin films have a high transparency (>90%) in the visible region, and high absorption (~100%) in ultraviolet region. The transmittance reduces slightly from 99% to 94% as the calcination temperature increase which is may result to the improvement of crystalline nature. The same observation was reported in previous works [19-21]. Notably, the interference fringes appear in the spectrum but not in sufficient manner to calculate the thickness with Swanepoel method, this was the main reason for choosing the gravimetric method for

thickness measurement. The low absorbance of ZnO thin films in the visible range of spectrum (~9%) makes these films suitable as a window layer in solar cells.

III.3.2.5.2 Band gap and Urbach energy:

The optical band gap E_g and Urbach energy E_u of the deposited thin film are shown in Table III-3, and traced in Figure III-10. The average value of the band gap it found to be 3.28 eV. It is observed that the band gap increases with increasing calcination temperature from 3,27 eV to 3,31eV in the range of [300-450°C], which might be caused by the improvement in crystal quality. This increase of band gap is confirmed by the decreasing in band tail width (Urbach energy) in the same range, the latter may be a result of the structural defects appearing in the film. K. Salim and M. N. Amroun, reported the same variation over the temperature range [300-400°C] [22].

Table III-3: Band gap and Urbach energy as function of the calcination temperature.

Temperature[°C]	**Band gap E_g**[eV]	**Urbach energy E_u**[eV]
300	**3.27**	**0.067**
350	**3.29**	**0.057**
400	**3.30**	**0.052**
450	**3.31**	**0.04**
500	**3.29**	**0.061**
550	**3.27**	**0.066**

Then for the high calcination temperature [500-550°C], the band gap decreases to 3.29 eV and 3,27 eV inversely with urbach energy. Narrowing of band gap with increasing calcination temperature may be attributed to the increase of carrier concentration according to the Burstein-Moss effect [23,24], since the absorption edge of degenerate semiconductor is shifted to shorter wavelength with increasing carrier concentration [24].

The band tail in the sample calcined at 300°C is 0.067 eV, which considered the highest value in the table; this is due to poor crystallinity in the low calcination temperature, which is in good agreement with XRD analysis. This means that as the calcination temperature decreases the influence of tailing on the band gap energy became larger.

It is clearly noticed that the film calcined at 450°C had the highest band gap and lowest urbach energy values, 3.31 eV and 0.04 eV, respectively.

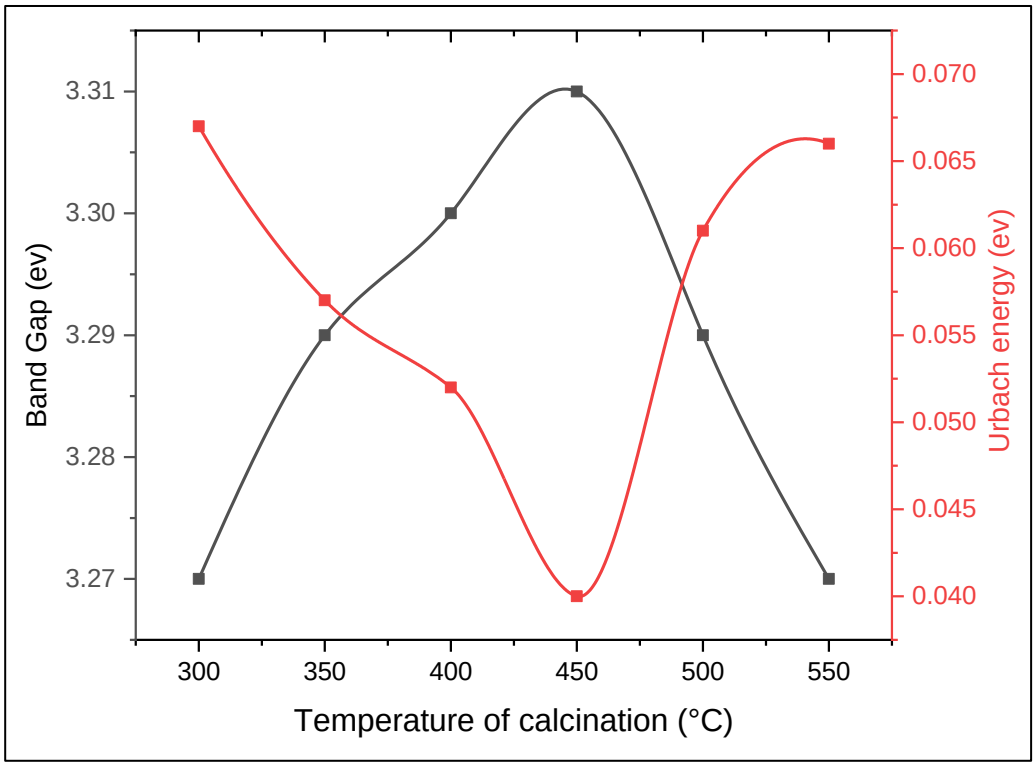

Figure III-10: Variation of band gap and Urbach energy versus the temperature of calcination.

III.3.2.5.3 Refractive index:

The refractive index of the film determined by Herve and Vandamme relation (II-21) are shown in Table III-4. Knowing that the refractive index has a strong relation with band gap, so it can be notice that it decreases with increasing the band gap, so it can be concluded that the smaller band gap energy material has a larger value of refractive index [18].

Table III-4: Refractive index values in function of temperature of calcination

Temperature °C	Refractive index (n)
300	**2.271**
350	**2.266**
400	**2.263**
450	**2.260**
500	**2.266**
550	**2.271**

As can be seen in Table III-4, the values of refractive index are almost the same, the average can be ~2.266, this is probably due to the low values of roughness taken from profilometry and the 3D images (Figure III-8), plus the slight reducing of transmittance shown in (Figure III-9).

III.3.2.6 Electrical characterization:

The variation of electrical conductivity and sheet resistance of ZnO films measured by four probes points method at various calcination temperatures can be found in Figure III-11 and Table III-5. It is well known that the electrical conductivity usually increases with increasing the temperature; this change can be seen in this Figure. And the sheet resistance changes inversely with conductivity.

Table III-5: Values of conductivity, sheet resistance and the resistivity of ZnO thin films samples calcined at various temperatures.

Temperature [°C]	**Moyenne R sheet [MΩ]**	**Resistivity [Ω. cm]**	**Conductivity [$(\Omega.\mathrm{cm})^{-1}$]**
400	**7.004000**	$\mathbf{2.619 \times 10^{2}}$	$\mathbf{3.817528 \times 10^{-3}}$
450	**8.655000**	$\mathbf{2.137 \times 10^{2}}$	$\mathbf{4.677739 \times 10^{-3}}$
500	**0.396566209**	**12.5711**	$\mathbf{7.9547225 \times 10^{-2}}$
550	**0.270772**	**7.2837**	$\mathbf{1.3729 \times 10^{-1}}$

It was difficult to characterize the electrical properties of the two samples calcined at 300°C and 350 °C due to its small thickness and poor crystalline nature, which implies that ZnO thin film have a deficient electrical property at low calcination temperature.

From the Table III-5, it seems that the conductivity value improved from $3.81 \times 10^{-3}(\Omega.\mathrm{cm})^{-1}$to $1.3729 \times 10^{-1}(\Omega.\mathrm{cm})^{-1}$with increasing calcination temperature in the range of [400-550 °C] which means that ZnO thin films have a good electrical property at high temperature which can be considered as a good semiconductor. Moreover, the sheet resistances of ZnO thin films decreased significantly from 7 MΩ to 0.27 MΩ when calcination temperature was raised. This recognizable change in these parameters usually depends of carrier concentration and mobility or one of them during the improvement of the crystallization quality [6].

The reasons for this variation in electrical properties can be explained simply as follows. The calcination process is conducive to the improvement of the crystallization's quality of the thin film (as

shown in XRD specters in Figure III-5). It may lead to the decrease of free electron scattering, which induces the increase of the carrier concentration and mobility. LinQ. et al., studied the effect of calcination temperature on ZnO thin films and they found that the mobility increases with increasing calcination temperature [25].

Also at high temperature, the non-stoichiometric cases can be formed by an excess of zinc atoms, or because of missing oxygen atoms from one of the lattice sites, which creates oxygen vacancies, these vacancies can results an excess of electrons, probably leads to the improvement of electrical conductivity at high calcination temperature. It is known that the vacancies considered as a defect, this proves the increasing of the Urbach energy at high temperature (Figure III-10).

As explained before, the reducing of optical band gap at high temperature may be due to Burstein-Moss effect [24]. At the same range of temperature [500-550°C] it was recorded a recognizable improvement in the electrical conductivity from the order of $10^{-3}(\Omega.\,\mathrm{cm})^{-1}$to $10^{-1}(\Omega.\,\mathrm{cm})^{-1}$. So, this increasing of electrical conductivity probably due to the increasing of carrier concentration which causes the increase in electron mobility.

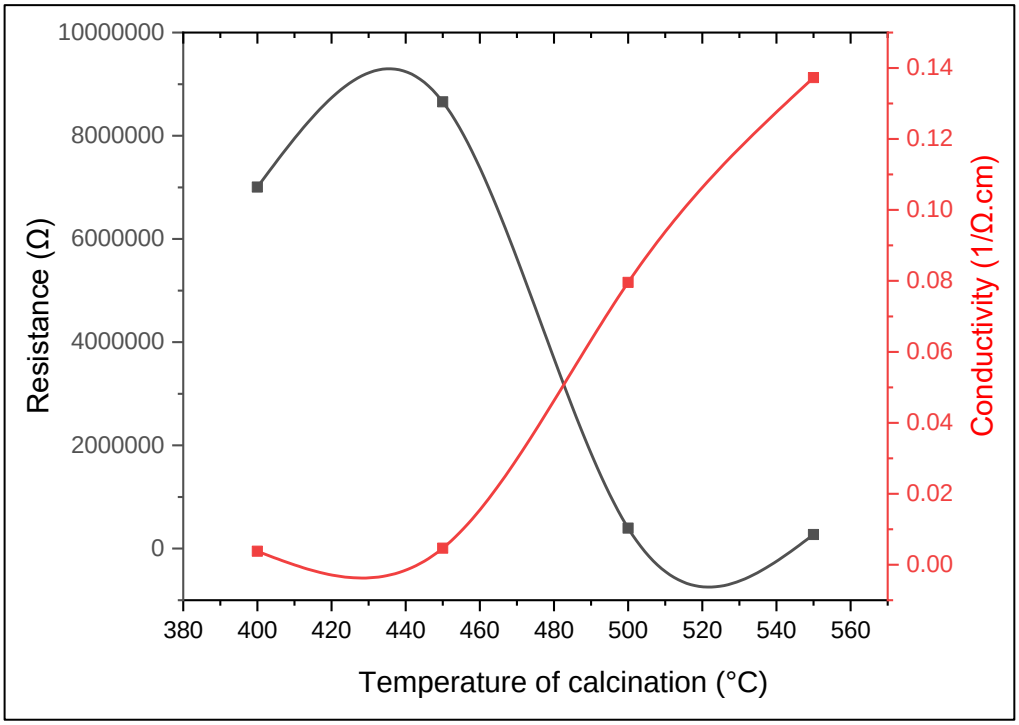

Figure III-11: Variation of R sheet and Conductivity in function of calcination temperature.

III.3.2.6.1 Figure of merit:

The figure of merit (FOM) is important to evaluate the performance of TCOs. The determined figure of merit can be found in Table III-6, it is common that this factor increases inversely with sheet resistance; this variation can be observed in this table. Generally, the values of this factor are low

comparing with the doped ZnO thin films, like ZnO:Al thin films, it was reported in literature [26,27] that FOM is in order of $10^{-4}$and 10^{-1} respectively.

We can observe that ZnO thin films calcined at 400 and 450 °C had low value of figure of merit, the main reason of that is the high value of resistance. It increases in recognizable way at high temperature of calcination, we can note that the thin film of ZnO calcined at 550°C had the highest value of figure of merit which means that it has the best performance, but not in sufficient way.

Table III-6: Values of sheet resistance and Figure of Merit of ZnO thin films calcined at various temperatures.

Temperature °C	R sheet (MΩ)	Figure of merit
400	**7.004000**	$\mathbf{1.36754 \times 10^{-7}}$
450	**8.655000**	$\mathbf{8.48514 \times 10^{-8}}$
500	**0.396566209**	$\mathbf{1.41411 \times 10^{-6}}$
550	**0.270772**	$\mathbf{2.89664 \times 10^{-6}}$

III.3.2.7 Calcination at 600°C:

The calcination temperature was planned to be reached to 600°C, but when the sample was removed from the furnace after 2 hours of calcination, we found a recognizable deformation on the substrate can be seen with the unaided eye. Because of this damage, it was difficult to characterize and compare the properties of this thin film with the other films.

The crystallite size of this sample has been calculated using the Debye–Scherer formula ((II-13), (II-14) in Chapter II) (Table III-7). These results should be deal in conservatively way.

Table III-7: Structural parameters values of ZnO thin films calcined at 600°C.

Temperatures [°C]	2θ [°]	FWHM	Crystallite size [nm]	d_{hkl}[Å]
600	**34.4792**	**0.3542**	**24**	**2.60128**

As can be seen in Figure III-13, an obvious deformation in XRD pattern, it can be confirmed in Figure III-14 which shows clearly curvature in transmittance spectrum.

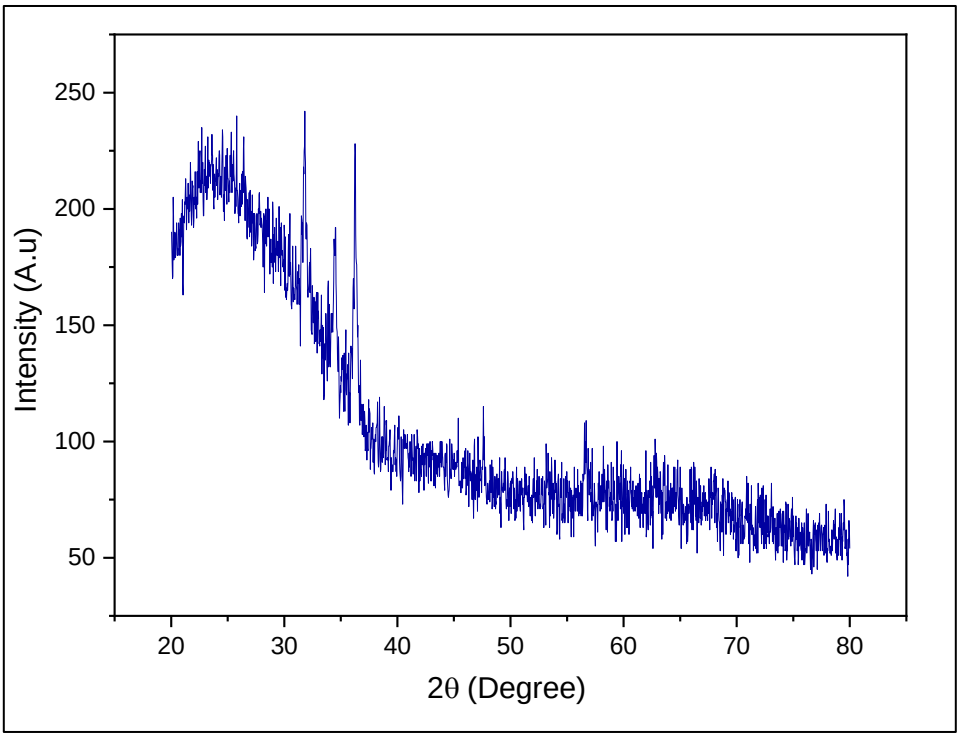

Figure III-13: XRD pattern of thin film ZnO calcined at 600°C.

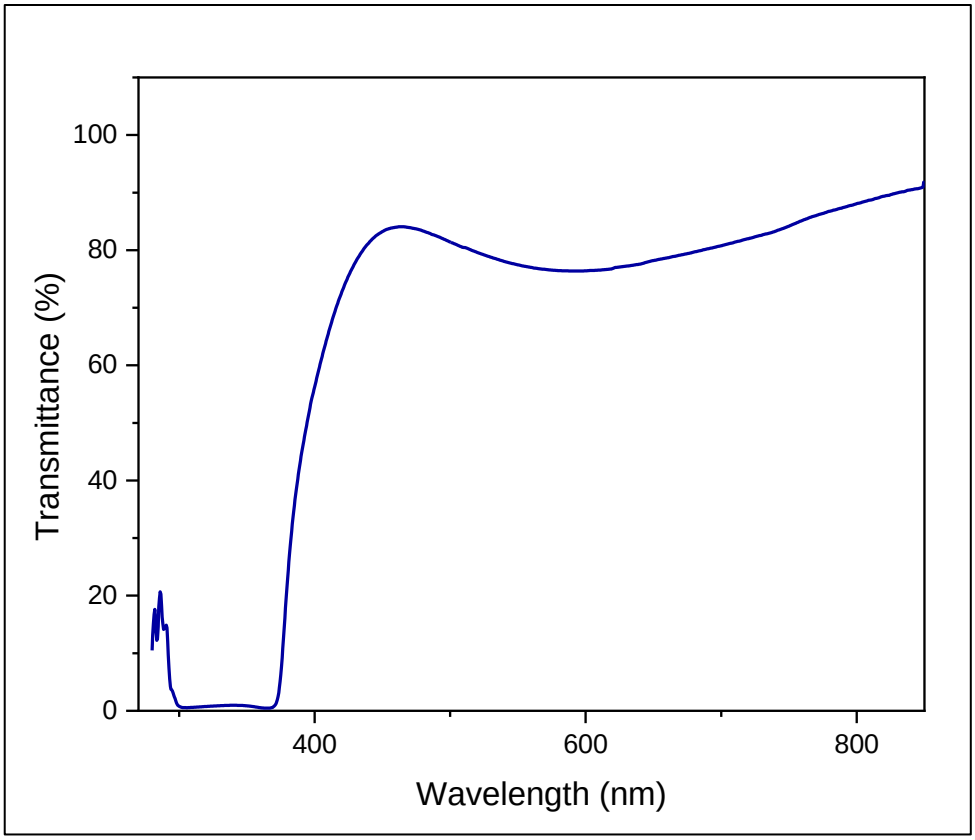

Figure III-14: Transmittance spectra of thin film ZnO calcined at 600°C.

REFERENCES

[1] F. Bouaichi, Deposition and analysis of Zinc Oxide thin films elaborated using spray pyrolysis for photovoltaic applications. Doctoral Thesis, University of Biskra, Algeria (2019).

[2] Saâd Rahmane, Elaboration et caractérisation de couches minces par spray pyrolyse et pulvérisation magnétron, Doctoral Thesis, Biskra University Algeria (2008).

[3] Kaufman & Robinson. Inc, In-Situ Cleaning for Thin-Film Deposition, Technical Note KRI TN-06, (2006).

[4] زوبيري بلال، دراسة خصائص الشرائح الرقيقة لأكسيد الزنك المحضرة بطريقة الرش بالهواء المضغوط انطلاقا من مصادر مختلفة للزنك، مذكرة ماستر، جامعة بسكرة، (2021).

[5] Holmarc Opto-Mechatronics. (2022). Dip Coating Unit with Infrared Dryer; https://www.holmarc.com/dip_coating_unit_IR.php.

[6] M. Firdaus Malek, M. Hafiz Mamat, M. Zahidi, M .Zainizan Sahdan, M. Rusop Mahmood,2013, Factors Affecting the Properties of Zinc Oxide Thin Films Prepared by Dip-Coating Method: A Review, Advanced Materials Research,667 (2013), 193-199.

[7] M. Firdaus Malek, M. Hafiz Mamat, M. Zahidi, M. Zainizan Sahdan, M. Rusop Mahmood, Calcinations Effect on Growth of Zinc Oxide Films prepared via Dip coating Technique, Advanced Materials Research, 1087 (2015), 374-378.

[8] A. Yahia, Optimization of indium oxide thin films properties prepared by sol gel spin coating process for optoelectronic applications, Doctoral Thesis, University of Biskra, Algeria (2020).

[9] M. Dahnoun, Preparation and characterization of Titanium dioxide and Zinc oxide thin films via Sol-Gel (spin coating) technique for optoelectronic applications. Doctoral Thesis, University of Biskra, Algeria (2019).

[10] Kat. Pesta, KIT – The Research University in the Helmholtz Association, (2021).

[11] M. Othmane, Synthesis and characterization of Zinc Oxide (ZnO) Thin films deposited by spray pyrolysis for applying: electronics and photonics. Doctoral Thesis, University of Biskra, Algeria (2018).

[12] S. Rahmane, M. A. Djouadi, Optoelectronic properties of ZnO thin films grown by radio frequency magnetron sputtering, Journal of Materials Science: Materials in Electronics, 31:17872–17878, (2020).

[13] R. Ghosh, G.K. Paul, D. Basak, Effect of thermal annealing treatment on structural, electrical and optical properties of transparent sol–gel ZnO thin films, Materials Research Bulletin 40 (2005) 1905–1914.

[14] N. Kouidri, S. Rahmane, A. Allag, Substrate temperature-dependent properties of sprayed cobalt oxide thin films, Journal of Materials Science: Materials in Electronics, 30 (2019):1153–1160.

[15] X.L. Zhang, K.S. Hui, Feng Bin, K.N. Hui, Lei Li, Y.R. Cho, R. S. Mane, Wei Zhou, Effect of thermal annealing on the structural, electrical and optical properties of Al–Ni co-doped ZnO thin films prepared using asol–gel method, Surface & Coatings Technology 261 (2015) 149–155.

[16] S. Rahmane, M.A. Djouadi, M.S. Aida, The effect of annealing on the properties of ZnO: Al films grown by Rf magnetron sputtering. Courrier du Savoir; N°18, (2014), 41-44.

[17] A. Allag, S. Rahmane, A. Ouahab, H. Attouche, N. Kouidri, Optoelectronic properties of SnO_2 thin films sprayed at different deposition times, Chinese Physical Society and IOP Publishing Ltd, Vol. 25, No. 4 (2016) 046801.

[18] A .Allag, S. Rahmane, N. Kouidri, H. Attouche, A. Ouahab, Polycrystalline SnO_2 thin films grown at different substrate temperature by pneumatic spray, J Mater Sci: Mater Electron, 28, (2017), 4772–4779.

[19] M. Arif, A. Sanger, M. Paula Vilarinho, A. Singh, Effect of Annealing Temperature on Structural and Optical Properties of Sol–Gel-Derived ZnO Thin Films, Journal of ELECTRONIC MATERIALS, Vacuum 155 (2018), 662–666.

[20] U. Chaitra, D. Kekuda , K. Mohan Rao, Effect of annealing temperature on the evolution of structural, microstructural, and optical properties of spin coated ZnO thin films. Ceramics International, 43(9), (2017)7115–7122.

[21] T. Ivanova, A. Harizanova, T. Koutzarova, B. Vertruyenc, Study of ZnO sol-gel films: Effect of annealing, Materials Letters, vol. 64, (2010).

[22] K. Salim, M. N. Amroun, Study of the Effects of Annealing Temperature on the Properties of ZnO Thin Films Grown by Spray Pyrolysis Technique for Photovoltaic Applications, J. Thin. Film. Sci. Tec. 11, No. 1, (2022)19-28.

[23] E. Burstein, Anomalous Optical Absorption Limit in InSb, Phys. Rev. 93, (1954)632.

[24] T. S. Moss, The Interpretation of the Properties of Indium Antimonide, Proceedings of the physical Society London B76 (1954) 775.

[25] Q. Lin, F. Zhang, N. Zhao, P. Yang, Influence of Annealing Temperature on Optical Properties of Sandwiched ZnO/Metal/ZnO Transparent Conductive Thin Films. Micromachines 13(2022) 296.

[26] J. Benny, P.K. Manoj, V.K. Vaidyan, Studies on the structural, electrical and optical properties of Al-doped ZnO thin films prepared by chemical spray deposition, Ceramics International, 32 (2006) 487–493.

[27] B. Sarma, D. Barman, K. Bimal Sarma, AZO (Al:ZnO) thin films with high figure of merit as stable indium free transparent conducting oxide, Applied Surface Science, 479, (2019) 786–795.

GENERAL CONCLUSION

GENERAL CONCLUSION

This work is based on elaboration and characterization of ZnO thin films by sol-gel via dip-coating technique on glasses substrate, and studying the influence of calcinations temperature on the various properties of these films. The structural properties of the deposited films have been analysed using X-ray diffraction (XRD). The optical properties are investigated by UV-VIS spectroscopy, and Profilometry results allow us to characterize the morphological properties, and the electrical properties have been obtained by four probes method.

The films have been calcined in a furnace at different temperatures (300, 350, 400, 450, 500 and 550 °C). The film thickness is measured by gravimetric method, which found to be less than $1\mu m$ and changes from 237 to 374 nm. X-ray diffraction study shows that all the films prepared in this work have polycrystalline hexagonal wurtzite structure with a preferential (002) orientation, raising the calcination temperature leads to increased crystallite size taking a highest value 46.9 nm at 550°C, while decreasing the strain in the films. The morphological observations indicated that the surface has a smooth and low roughness; increasing the calcination temperature influenced the surface roughness and raises the values of RMS.

The prepared ZnO thin films have a good optical property, with high transparency in the visible range around ~97%. The average value of the band gap it found to be 3.28 eV, and Urbach energy in order of 60 meV, which indicate the low defects in these films. The refractive index of ZnO thin films, has been found to be almost ~2.266. When the calcination temperature increases from 400 to 550°C we have observed that there is a recognizable increment in the value of the electrical conductivity of ZnO films, it was from 3.8×10^{-3} to $1.37 \times 10^{-1} (\Omega . \mathrm{cm})^{-1}$, respectively, which indicate the good electrical quality of these films at high temperature. In addition, we determined the figure of merit it was in order of 10^{-6} at 550°C, which presents an acceptable performance of transparent conductive oxide (TCO).

In summary, we found that the calcination temperature is an important parameter which influenced the ZnO thin films properties. The best results are reached at the high calcination temperature, such as the structural and optical properties like crystallite size and transparency, the morphological like roughness, and the electrical conductivity. The film prepared at this temperature are considered the most promising as n-type semiconductor films for technological applications such as transparent layers in solar cells.

ABSTRACT

The influence of calcination temperature on properties of thin films of Zinc-Oxide (ZnO) elaborated by Sol-gel (Dip-coating)

In the present work; we used Sol-Gel Dip-coating technique to deposit Zinc oxide thin films, and studied the influence of the calcination temperature on the structural, morphological, optical and electrical properties. As well as, all the ZnO thin films were characterized by multiple techniques such as X-ray diffraction, UV-visible spectroscopy, Profilometry and Four probes method.

Our main objective is to optimize the properties by varying the calcination temperature; we observed that film calcined at high temperature of $550°C$ has the best crystallization like crystallite size about 46.9 nm, transmittance$\sim 97\%$ and conductivity $1.37 \times 10^{-1}(\Omega.\,\mathrm{cm})^{-1}$, although the surface morphology has a smooth and low roughness.

Keywords: ZnO, thin films, sol-gel, dip-coating, calcination, temperature, properties.

RESUME

L'influence de la température de calcination sur les propriétés des couches minces d'oxyde de zinc (ZnO) élaborés par Sol-gel (Dip-coating)

Dans ce présent travail on a utilisé la technique Sol-gel Dip-coating pour déposer des couches minces d'oxyde de zinc, et étudie l'influence de la température de calcination sur les propriétés structurale, morphologique, optique et électrique. Pour cela, les couches minces de ZnO ont été caractérisées par multiples techniques telles que la diffraction de rayon X (DRX), UV-visible spectroscopie, profilométrie et quatre pointes.

Notre objectif principal est d'optimiser les propriétés en fonction de la température de calcination ; nous avons observé que le film calciné à haute température 550°C a la meilleure cristallisation comme la taille de cristallite était 46.9 nm, la transmittance$\sim 97\%$, la conductivité $1.37 \times 10^{-1}(\Omega.\,\mathrm{cm})^{-1}$, bien que la morphologie de surface soit lisse et a une faible rugosité.

Mots clés : ZnO, couches mince, sol-gel, dip-coating, calcination, température, propriétés.